# The 1974 flank eruption of Mount Etna: An archetype for deep dike-fed eruptions at basaltic volcanoes and a milestone in Etna's recent history

R. Corsaro, N. Métrich, Patrick Allard, D. Andronico, L. Miraglia, C. Fourmentraux

# The 1974 flank eruption of Mount Etna: An archetype for deep dike-fed eruptions at basaltic volcanoes and a milestone in Etna's recent history

R. A. Corsaro,[1] N. Métrich,[2,3] P. Allard,[1,2] D. Andronico,[1] L. Miraglia,[1] and C. Fourmentraux[2,4,5]

Received 14 August 2008; revised 29 January 2009; accepted 4 May 2009; published 22 July 2009.

[1] The 1974 western flank eruption of Mount Etna produced a rare, nearly aphyric and plagioclase-free trachybasalt that could not be derived from the central volcano conduits and was more alkaline and more radiogenic than all previous historical lavas. New results for the petrochemistry and volatile content of its products, combined with contemporaneous seismic and volcanological observations, allow us to reinterpret the origin and significance of this event. We show that the eruption was most likely triggered by deep tectonic fracturing that allowed a dike-like intrusion to propagate in 9 days from $\geq$11 km depth up to the surface, bypassing the central conduits. Relatively fast, closed system decompression of the volatile-rich magma initially led to lava fountaining and the rapid growth of two pyroclastic cones (Mounts De Fiore), followed by Strombolian activity and the extrusion of viscous lava flows when gas-melt separation developed in the upper portion of the feeding fracture. The 1974 trachybasalt geochemistry indicates its derivation by mixing 25% of preexisting K-poor magma (best represented by 1763 La Montagnola eruption's products) and 75% of a new K-rich feeding magma that was gradually invading Mount Etna's plumbing system and became directly extruded during two violent flank eruptions in 2001–2003. We propose to classify 1974-type so-called ''eccentric'' eruptions on Etna as deep dike-fed (DDF) eruptions, as opposed to more common central conduit-fed flank eruptions, in order to highlight their actual origin rather than their topographic location. We ultimately discuss the possible precursors of such DDF eruptions.

**Citation:** Corsaro, R. A., N. Métrich, P. Allard, D. Andronico, L. Miraglia, and C. Fourmentraux (2009), The 1974 flank eruption of Mount Etna: An archetype for deep dike-fed eruptions at basaltic volcanoes and a milestone in Etna's recent history, *J. Geophys. Res.*, *114*, B07204, doi:10.1029/2008JB006013.

## 1. Introduction

[2] Mount Etna, the most active volcano in Europe, is a large (40 km wide and 3.3 km high) basaltic stratovolcano that has been built since 0.5 Ma in eastern Sicily, at the intersection of tensional tectonic fractures that cut the locally ~20 km thick African continental margin. Like other well developed active basaltic volcanoes, such as Kilauea (Hawaii), Klyoutchevskoi (Kamchatka) and Izu-Ozima (Japan), Mount Etna produces both summit and flank eruptions that are principally controlled by magma rise in well established central conduits [e.g., *Rittmann*, 1965; *Wadge*, 1980; *Ryan*, 1988; *Chester et al.*, 1985; *Allard et al.*, 2006]. Summit eruptions take place at the open exit (summit craters) or subterminal branching of these central conduits, and are much more common than flank eruptions [*Branca and Del Carlo*, 2004; *Allard et al.*, 2006]. However, the relatively high frequency of the latter is attested by the presence of 338 monogenetic cones of varying age on the volcano slopes (see *Armienti et al.* [2004] for a review), preferentially concentrated along the main volcano-tectonic structures of regional direction that have controlled the volcano build up (Figure 1a). The flank eruptions can happen at low elevation and produce lava flows of sometimes considerable extent, thereby constituting a major hazard for the densely populated surroundings. Most of these events are typically driven by fracturing of the central conduits and radial magma drainage across the volcanic pile. Indeed, their erupted lavas are analogous to those erupted from the summit craters in being highly porphyritic (~30–40% crystals) and prevalently rich in plagioclase phenocrysts which increasingly develop in response to water degassing in the central conduits [*Métrich and Rutherford*, 1998; *Métrich et al.*, 2004]. Conduit fracturing and lateral drainage of the crystal-rich conduit magma can be triggered by magmatic

[1]Istituto Nazionale di Geofisica e Vulcanologia, Catania, Italy.
[2]Laboratoire Pierre Süe, UMR 9956, CEA, CE-Saclay, CNRS, Gif-sur-Yvette, France.
[3]Istituto Nazionale di Geofisica e Vulcanologia, Pisa, Italy.
[4]Now at Dipartimento di Scienze della Terra, Pisa, Italy.
[5]Now at Istituto Nazionale di Geofisica e Vulcanologia, Pisa, Italy.


0148-0227/09/2008JB006013$09.00

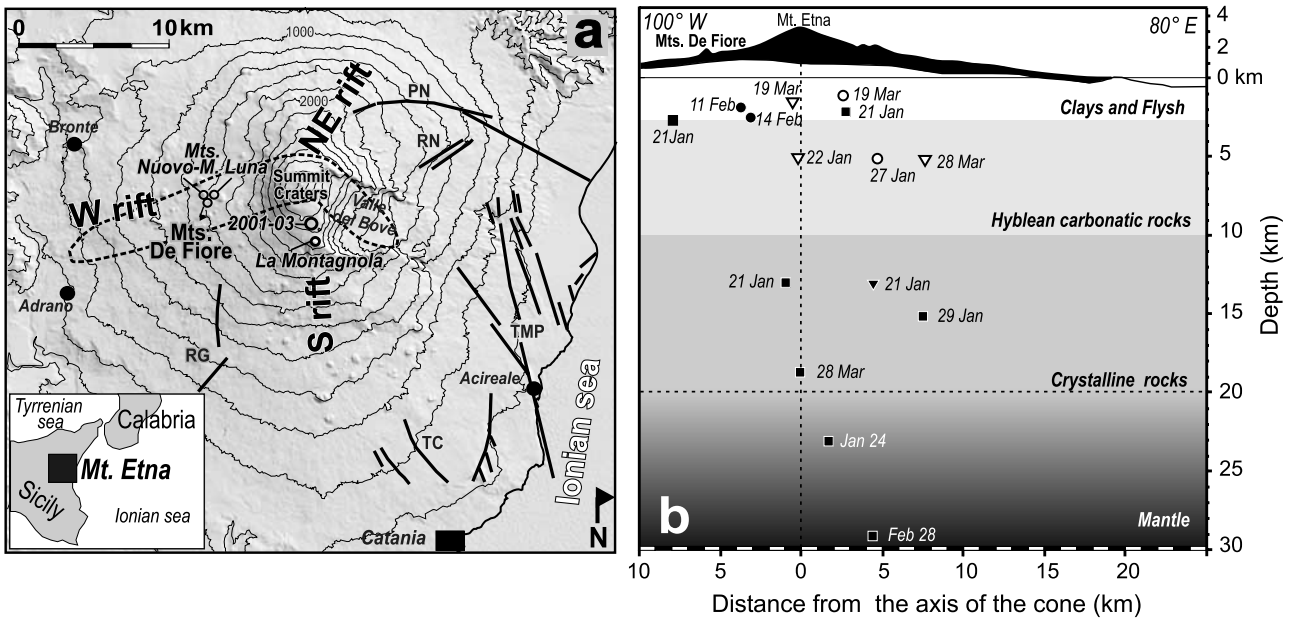


**Figure 1.** Location of the 1974 western flank (Mounts De Fiore) eruption of Etna and spatial distribution of the associated preeruptive and syneruptive seismicity. (a) Digital map of Mount Etna showing its main volcano-tectonic structures (rifts zones and fault systems) and the locations of the 1974, 1763 (La Montagnola), 2001, 2002–2003, and Mount Nuovo–Mount Mezza Luna flank eruptions vents (modified from *Allard et al.* [2006]). The dashed lined area shows the main ENE–WSW epicentral distribution of earthquakes with magnitude >3 that occurred before and during the 1974 flank eruption (data from *Bottari et al.* [1975]). Main fault systems: PN, Pernicana; RN, Ripe della Naca; TMP, Timpe; TC, Trecastagni; RG, Ragalna. The regional setting of Mount Etna is shown in the inset. (b) Hypocenter distribution of the most energetic earthquakes before and during the 1974 eruption [*Bottari et al.*, 1975]. The reliability of earthquake locations is indicated by either full symbols (good) or open symbols (approximate), and different symbols define classes of magnitude (M): $M \geq 4$ (square), $4 > M \geq 3.5$ (triangle) and $3.5 > M \geq 2$ (circle) [*Bottari et al.*, 1975]. The stratigraphy of Etna's crustal basement is summarized from *Chiarabba et al.* [2004] and *Corsaro and Pompilio* [2004, and references therein]. The most energetic and deepest earthquakes delineate a 70° inclined western border for the activated seismogenic volume that connects the flank eruption site to the base of the crust (see text).

overpressure but also volcano flank instability, regional tectonic stress variations or a combination of these [e.g., *Rittmann*, 1965; *Chester et al.*, 1985; *Acocella and Neri*, 2003; *Allard et al.*, 2006].

[3] However, a few rare flank eruptions of Etna do not belong to the above category. In addition to being highly explosive, these events emitted a nearly aphyric magma, devoid of any plagioclase phenocrysts, which therefore underwent only minor water degassing and crystallization prior to erupting. In historical times, the only know examples of such eruptions occurred in 1763 [*Sturiale*, 1970; *Miraglia*, 2002], 1974 [*Bottari et al.*, 1975; *Tanguy and Kieffer*, 1977], 2001 [*Métrich et al.*, 2004; *Corsaro et al.*, 2007] and 2002–2003 [*Andronico et al.*, 2005; *Spilliaert et al.*, 2006]. It is obvious that these events were not fed from the central conduits. Instead, they must have been driven by deeply rooted intrusions, generated from below the volcanic pile, which bypassed the central conduits while propagating upward. Such eruptions were termed "eccentric" [*Rittmann*, 1965] or "peripheral" [*Acocella and Neri*, 2003]. However, such topographical terminologies are confusing because some of these events can break out in the subterminal part of the volcano and close to the central conduits (e.g., the 2002–2003 eruption, 2800 m above sea level (asl); Figure 1a). Therefore, in this work we propose to classify this type of flank events as "deep dike-fed" (DDF) eruptions, as opposed to more common "central conduit-fed" (CCF) eruptions, in order to better characterize their main attribute: their supply by intrusions that originate from below the volcanic pile and that bypass the central conduits.

[4] In this paper we focus on the January–March 1974 flank eruption of Etna that, as we show thereafter, can be considered as an archetype for DDF-type flank events. This eruption was unusual in several aspects: it was preceded and accompanied by one of the most intense volcano-tectonic seismic crisis ever registered on Etna (600 recorded earthquakes, many of them felt, and nine of which with magnitude $\geq 4$ [*Bottari et al.*, 1975; *Guerra et al.*, 1976]); it was highly explosive and developed in two phases of similar length and pattern, separated by as much as 22 days; and its erupted aphyric magma markedly differed from all previous historical Etnean lavas in being enriched in potassium and other alkalis [*Bottari et al.*, 1975; *Tanguy and Kieffer*, 1977; *Clocchiatti et al.*, 1988; this work], $^{226}$Ra [*Condomines et al.*, 1987, 1995] and both radiogenic strontium and boron isotopes [*Tanguy et al.*, 1997; *Tonarini*

*et al.*, 2001]. In the past, Mount Etna had occasionally erupted alkali-enriched magmas during the Holocene (Mount Maletto basalt, 7 ka [*Kamenetsky and Clocchiatti*, 1996; *Schiano et al.*, 2001]) and then at 3930 ± 60 years B.P. (FS picritic basalt [*Coltelli et al.*, 2005; *Kamenetsky et al.*, 2007]). But the 1974 flank eruption revealed the first known extrusion of such a magma type in historical times. Furthermore, this event happened in broad coincidence with a sharp increase in Etna's eruption frequency and explosivity, in the bulk magma extrusion rate [e.g., *Andronico and Lodato*, 2005; *Allard et al.*, 2006], and was actually followed by a progressive potassium enrichment of Etna lavas in the next decades that culminated in voluminous extrusion of a closely similar K-rich trachybasalt during two DDF-type flank eruptions in 2001 then 2002–2003 [*Clocchiatti et al.*, 2004; *Métrich et al.*, 2004; *Andronico et al.*; 2005; *Spilliaert et al.*, 2006; *Viccaro et al.*, 2006; *Corsaro et al.*, 2007].

[5] Paradoxically, despite its singularities little attention has been paid to the 1974 flank eruption since early reports and publications in the mid-1970s [*Guest et al.*, 1974; *Tazieff*, 1974; *Working Group for the Surveillance of Etna*, 1974; *Bottari et al.*, 1975; *Tanguy and Kieffer*, 1977; *Guerra et al.*, 1976]. Moreover, in these reports contradictory interpretations were proposed for its origin, some authors favoring its shallow derivation [*Guest et al.*, 1974; *Bottari et al.*, 1975; *Guerra et al.*, 1976] and others its direct feeding from mantle depths [*Tanguy and Kieffer*, 1977]. Therefore, for all these reasons we decided to carry out new investigations of this important event, in order to get improved understanding of its genesis and significance for the recent volcano evolution.

[6] Here we report new analyses of solid products from both the 1974 flank eruption and contemporaneous summit crater activity, sampled at that time by R. Romano [*Bottari et al.*, 1975; R. Romano, unpublished data, 1974] and more recently by ourselves. In addition to further determinations of their mineralogy and bulk rock major and trace element compositions, we provide the first data for the chemical composition and the volatile content of melt inclusions entrapped in olivine crystals of the 1974 flank trachybasalt. We also report similar new data for aphyric basaltic products from the June–August 1763 "La Montagnola" eruption, which best represent the K-poor magmas emitted in the previous centuries. Our results provide an updated evaluation of the solid and volatile budget the 1974 flank eruption and quantitative assessment of the depth and dynamics of ascent of its trachybasaltic magma. Combined with contemporaneous volcanological observations and data for the preeruptive and syneruptive seismicity [*Bottari et al.*, 1975; *Guerra et al.*, 1976], they allow us to propose a new interpretation of its triggering mechanism. We then examine the significance of the 1974 event with respect to recent changes in Etna's feeding system, by comparing its singular magma geochemistry to that of aphyric products from the 1763 and 2001–2003 DDF-type eruptions. Finally, we briefly discuss the volcanic risks posed by DDF-type flank eruptions on Etna and their possible precursors.

## 2. The 1974 Flank Eruption and Its Precursors

### 2.1. Etna's Previous Activity

[7] Prior to its 1974 flank eruption, Mount Etna was weakly to moderately active. After a CCF-type flank eruption in April–June 1971 ($75 \times 10^6$ m$^3$ of magma [*Rittmann et al.*, 1971]), which closed a period of intense explosive eruptive activity at the Northeast summit crater, the volcano had remained in almost complete quiescence for three months. In September 1971 spasmodic Strombolian-type activity resumed at the bottom of the Voragine central crater, associated with occasional emissions of altered lithic ashes. This same activity continued in 1972–1973, accompanied by crater wall collapses and alternated Strombolian outbursts inside the Voragine and Bocca Nuova craters [*Bottari et al.*, 1975]. In October–November 1973 the activity gradually increased, waxing with lava fountains at Voragine crater on 6 November, then waning once again. In December1973 to January 1974, weak Strombolian-type explosions, producing modest amounts of incandescent material but common ash emissions, were prevailing inside the Voragine crater. Crater wall collapses were also frequent. In the same time, the registered seismic activity was low and typically linked to the summit volcanic phenomena [*Bottari et al.*, 1975].

### 2.2. Precursory Seismicity

[8] On 20 January 1974, 10 days prior to the eruption onset, a violent seismic crisis began to be felt on the medium-low western side of the volcano, between the cities of Adrano and Bronte (Figure 1a). This crisis was strong enough to be recorded by permanent seismic stations in both Catania and Messina (70 km north of Etna). Although the seismic network was very limited at that time, its prompt complement with two more permanent stations (Serra la Nave and Monte Vetore) and mobile seismographs provided by alerted Italian teams allowed quite reasonable estimations of the earthquakes' epicenters (±1–4 km) and hypocenters (±2–5 km) during the January–April period of interest [*Bottari et al.*, 1975; *Working Group for the Surveillance of Etna*, 1974; *Guerra et al.*, 1976].

[9] The seismic crisis started at shallow (~2–3 km) depth and with moderate energy under the low western flank of Etna, but rapidly increased in magnitude and focal depth (~13–15 km) during the first 36 h while migrating toward the center of the volcano along an WSW–ENE (260°N) radial axis [*Bottari et al.*, 1975] (Figure 1a). The highest seismic energy release, with several earthquakes of magnitude between 3.4 and 4.3, occurred on 21 January. It coincided with a temporary but sudden drop of the magma column in the summit craters [*Bottari et al.*, 1975]. The deepest earthquake (23 km, M = 4.2) was recorded on 24 January. As illustrated in Figures 1a and 1b, during that preeruptive period and afterward, most of the earthquakes appeared to be concentrated within a WSW–ENE orientated seismogenic volume that extended, horizontally, from the low western flank to the summit craters and, vertically, from the shallow sedimentary basement (0.5 km asl to 2 km below sea level (bsl)) down to the base of the crust (~20–25 km bsl). The focal depths of the most energetic and deepest earthquakes delineated a 70° inclined western border for this seismogenic volume [*Bottari et al.*, 1975], connecting the base of the crust to the future eruption site (Figure 1b), which corresponds to a main pathway for Etna magma ascent within and along a huge plutonic body emplaced in the crustal basement [*Hirn et al.*, 1991; *Patanè et al.*, 2002; *Chiarabba et al.*, 2000, 2004]. Just NE of the summit craters

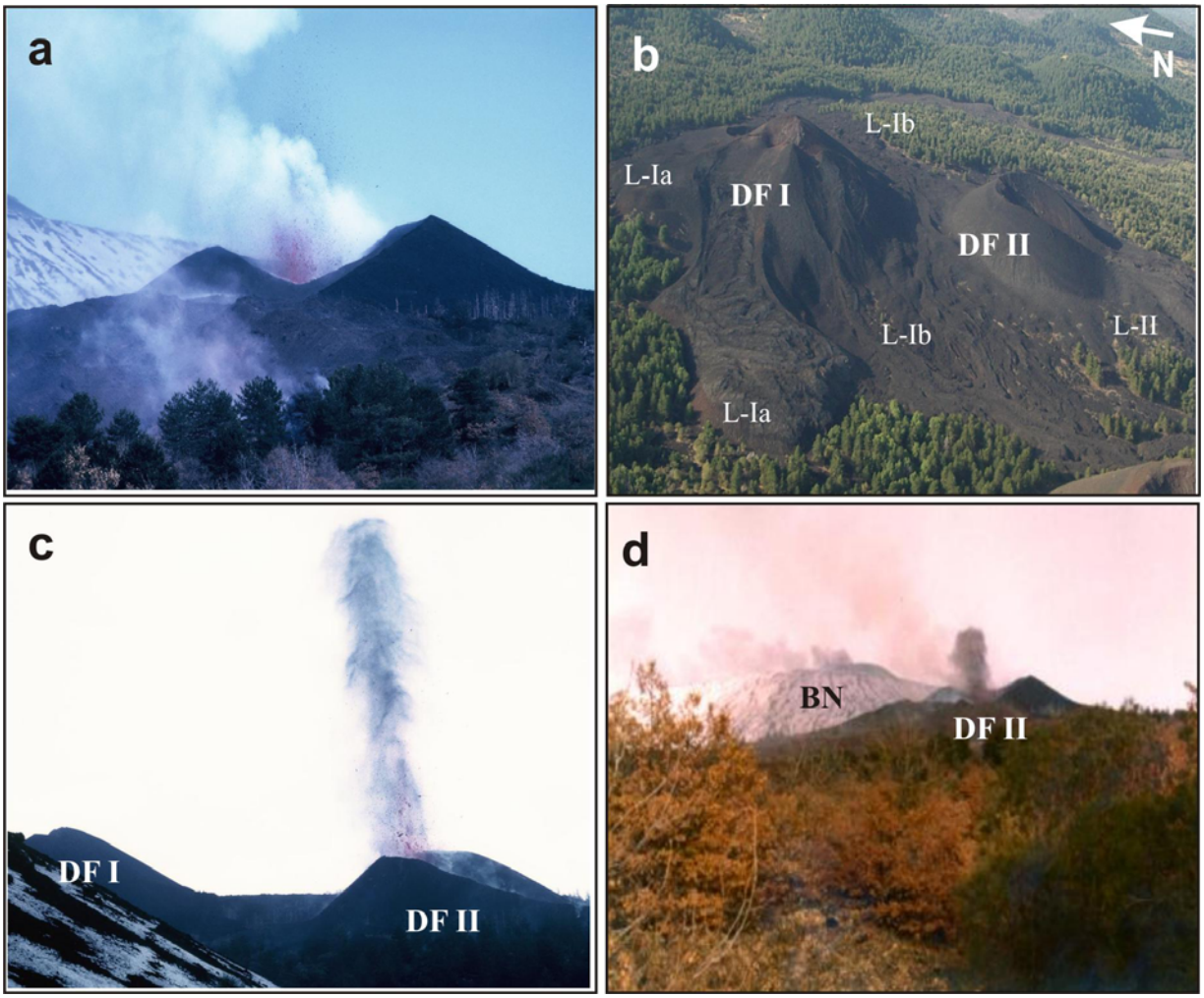


**Figure 2.** (a) View of Mount De Fiore I cone from the west: Strombolian explosions are ejecting bombs and ash. Snapshot from B. Puglisi. (b) Present aerial view of the 1974 eruptive vents. Abbreviations are DFI and DFII for Mount De Fiore cones I and II, respectively; L-Ia, Ib for lava flows erupted between 30 January and 12 February and then between 13 and 16 February; L-II for lava flows erupted between 11 and 29 March. (c) View of Mount De Fiore II from the northeast: the Strombolian activity causes a vertical, narrow ejection of incandescent scoria and blocks associated with a low, rising ash plume. In rear, Mount De Fiore I. Snapshot from B. Puglisi. (d) Ash emissions from the Bocca Nuova summit crater (BN) occurring in coincidence to Strombolian activity at Mount De Fiore II (DFII) in March 1974. Snapshot from C. Sturiale.

the main WSW–ENE seismic domain was connecting to another NW–SE (320°N) seismogenic axis, defined by a few energetic earthquakes with intermediate (13–15 km) depths [*Bottari et al.*, 1975]. A significant drop in seismic energy release coincided with the eruption outbreak.

### 2.3. Flank Eruption

[10] The 1974 eruption took place at quite low altitude (1670–1650 m asl) on the western flank of Etna (Figure 1a), in a sector where numerous monogenetic pyroclastic cones are aligned on a 240–260°N "west rift" [*Mazzarini and Armienti*, 2001, and reference therein]. The most recent eruptions in that sector had occurred in February–March 1763 (Mount Nuovo and Mount Mezza Luna), 1832 (Mount Nunziata) and 1843 [*Branca and Del Carlo*, 2004]. The 1974 eruption developed in two distinct phases, from 30 January to 17 February and then from 11 to 29 March [*Guest et al.*, 1974; *Tazieff*, 1974; *Working Group for the Surveillance of Etna*, 1974; *Bottari et al.*, 1975; *Tanguy and Kieffer*, 1977]. Below we summarize its most relevant features.

#### 2.3.1. First Eruptive Phase Mount De Fiore I

[11] At about 0500 LT on 30 January, an eruptive vent opened 6 km west of the summit craters (Figure 1a). Throughout the first day, almost continuous lava fountaining 150–400 m in height arose from that vent [*Tazieff*, 1974], building up a new pyroclastic cone (Mount De Fiore I, Figure 2a). The seismic tremor amplitude was the highest during this initial phase [*Guerra et al.*, 1976]. In the next days, fountaining was replaced by powerful explosions (30–50 per minute) which could hurl lava clots of a few kilograms to 300–500 m height and blocks of several tons to 100 m above the crater rim [*Tazieff*, 1974]. This change in activity was reflected in a clear drop of the seismic tremor [*Guerra et al.*, 1976], but led to a rapid growth of the new

cone to 70 m height in only about 3 days. In the same time, short-lived, rather viscous and thick lava tongues began issuing from 4 to 5 vents which successively opened at the base of the new cone. This explosive activity, associated with loud detonations and felt earth tremors, culminated in intensity and height (500–600 m) on 4–5 February. By 7–8 February explosions started to become more irregular and less intense, despite strong resumption from time to time, while lava flow outpourings became more important than at the beginning of the eruption. The largest flow (100 m wide, 1.5 km long) of this eruption was emitted on 8 February (Figure 2b). After a brief rest on 9 February, Strombolian explosive activity continued with a lower energy (~100–150 m height) until 12 February. Afterward the lava explosions were progressively replaced by more and more intermittent ash-laden outbursts, due to a lowering of the magmatic pressure. All explosive activity stopped on 16 February and a 1 km long lava flow was ultimately developed by 17 February.

[12] This 17-day-long first eruptive phase was accompanied by relatively modest seismic energy release, under the form of seismic tremor, explosion quakes and volcano-tectonic earthquakes with impulsive P arrival, high predominant frequency (5 Hz) and clear S phase [*Working Group for the Surveillance of Etna*, 1974; *Bottari et al.*, 1975; *Guerra et al.*, 1976]. However, its end was marked by a series of shallow but quite energetic seismic shocks felt in the sectors of Adrano, Bronte, and Ragalna (RG, Figure 1a) [*Bottari et al.*, 1975].

#### 2.3.2. Second Eruptive Phase Mount De Fiore II

[13] After 9 days of rest, a second seismic crisis began on 26 February under the same western–southwestern flank of the volcano (Figure 1a). This second preeruptive seismic sequence was relatively less intense than the first one, but had almost the same duration and occurred over a comparable depth range [*Bottari et al.*, 1975]. The deepest earthquake (29 km), with estimated magnitude 4.3, occurred on 28 February slightly east beneath the summit craters. On 11 March, a new eruptive vent opened only 200 m west of Mount De Fiore I. During the first 2 days, lava jetting and fountaining ejected coarse lapilli and scoria to 500–600 m height, leading to the rapid growth of a new horseshoe-shaped pyroclastic cone (Mount De Fiore II, Figures 2b and 2c). In the following days, the activity mostly consisted of powerful Strombolian explosions producing ash, scoria and coarse lava blocks (Figure 2c), while a series of viscous lava tongues issued from the crater breach. After a few days of irregular and less frequent explosions (from 80 to 50 per minute on 13 March), fountain activity resumed in coincidence with felt seismic shocks. It peaked on 19–22 March when the fountains were up to 500 m high and the ejected coarse material was falling up to 800 m from the vent [*Bottari et al.*, 1975]. After 23 March, the explosive activity markedly decreased in intensity (250 to 100 m high jets) and the conduit walls of the cone were seen to collapse intermittently. During the following days, lava explosions gradually alternated with powerful ash emissions. On 26–28 March, a brief but strong seismic swarm (including an earthquake with M = 4.3, located at 18 km depth; Figure 1b) coincided with the terminal stage of the eruption, marked by an ultimate expulsion of old coarse ash on early 29 March. This second eruptive phase thus had a similar duration (18 days) as the first one.

### 2.4. Contemporaneous Activity at the Summit Craters

[14] Volcanic activity at the Bocca Nuova and Voragine summit craters revealed some relationships with the seismo-volcanic phenomena related to the 1974 flank eruption. Of prime interest are the observed drops of the magma column in the summit vents that coincided with the highest initial preeruptive seismicity (21 January) and then with the earthquake shocks at the end of the eruption on 28 March [*Guest et al.*, 1974; *Bottari et al.*, 1975]. Moreover, during the first eruptive phase (DFI) quite continuous forceful ash expulsions and muffled explosions with deep (several hundred meters) origin occurred at the Voragine central crater [*Guest et al.*, 1974; *Bottari et al.*, 1975]. Again, during the second eruptive phase (DFII) continuous and occasionally violent ash emissions (Figure 2d) occurred at the Bocca Nuova (15–21 and 25–26 March), and noticeable fracturing cut the floor of the Voragine. On 24 March glowing was visible inside the Voragine and incandescent scoria were ejected from the Bocca Nuova [*Tanguy and Kieffer*, 1977; R. Romano, unpublished notes, 1974].

### 2.5. Eruption Magma Budget

[15] The cumulative volume of lava flows produced by the 1974 flank eruption was quantified as $4.5 \times 10^6$ m$^3$ by *Bottari et al.* [1975] and *Tanguy and Kieffer* [1977], with $2.4 \times 10^6$ and $2.1 \times 10^6$ m$^3$ outpoured during the DFI and DFII, respectively, eruptive phases (Table 1). For a mean flow vesicularity of about 20% this implies an equivalent dense magma volume of $3.6 \times 10^6$ m$^3$.

[16] The amount of erupted pyroclastites has been approximated by the combined volume of the Mount De Fiore I and II scoria cones. Initial estimates for these two pyroclastic cones were $1.8 \times 10^6$ m$^3$ and $0.9 \times 10^6$ m$^3$, respectively [*Bottari et al.*, 1975; *Tanguy and Kieffer*, 1977], but our field measurements, together with the model of *Riedel et al.* [2003] applied to the cones morphology, lead us to reassess their volume as $2.48 \times 10^6$ m$^3$ and $0.74 \times 10^6$ m$^3$ (Table 1). The additional deposit of coarse pyroclastites outside the cones was evaluated as $\sim 0.3 \times 10^6$ m$^3$ [*Bottari et al.*, 1975]. The amount of fine tephra is more difficult to estimate, owing to poor preservation of their deposits. However, it likely represents a minor contribution since the lack of a true eruption column during both DFI and DFII eruptive phases restricted ash fallout to within the immediate (~1–2 km) surroundings of the vents. Therefore, our updated estimate for the bulk amount of pyroclastites produced by the 1974 eruption is $3.52 \times 10^6$ m$^3$. For a mean scoria vesicularity of about 50%, this represents a dense equivalent magma volume of $1.76 \times 10^6$ m$^3$.

[17] The total volume ($5.4 \times 10^6$ m$^3$) and average eruption rate (1.8 m$^3$ s$^{-1}$) of dense magma produced over the 35-day duration of the 1974 eruption (Table 1) make it an event of relatively small magnitude. However, given the high volumetric proportion of tephra, its mean explosivity index (0.44) was anomalously high for an eruption on Etna [*Romano and Sturiale*, 1982; *Andronico and Lodato*, 2005]. It is also worth noting that the first eruptive phase was about twice as explosive (0.53) and productive

**Table 1.** Volcanological Parameters and Budget of the 1974 Flank Eruption of Mount Etna

| | DFI Phase | DFII Phase | Total |
|---|---|---|---|
| Date | 30 Jan to 17 Feb | 11–29 Mar | |
| Duration (days) | 17 | 18 | 35 |
| Vent altitude (m asl) | 1670 | 1650 | |
| *Lava Flows*[a] | | | |
| Maximum lava flow length (km) | 1.5 | 1.3 | |
| Average thickness (m) | 8.0 | 10.5 | |
| Covered area ($km^2$) | 0.3 | 0.2 | 0.5 |
| Lava volume ($10^6$ $m^3$) | 2.4 | 2.1 | 4.5 |
| Mean effusion rate ($m^3$ $s^{-1}$) | 1.6 | 1.35 | 1.5 |
| *Pyroclastites* | | | |
| Mount De Fiore scoria cone[b] ($10^6$ $m^3$) | 2.5 | 0.75 | 3.25 |
| Proximal tephra depth[a] ($10^6$ $m^3$) | 0.2 | ~0.1 | 0.3 |
| Mean eruption rate ($m^3$ $s^{-1}$) | 1.8 | 0.55 | 1.2 |
| First 3-day bulk eruption rate[c] ($m^3$ $s^{-1}$) | 9.2 | 3.1 | |
| Explosivity index[d] | 0.53 | 0.29 | 0.44 |
| *DRE Magma*[e] | | | |
| Lava flows ($10^6$ $m^3$) | 1.9 | 1.7 | 3.6 |
| Pyroclastites ($10^6$ $m^3$) | 1.35 | 0.42 | 1.8 |
| Bulk volume ($10^6$ $m^3$) | 3.25 | 2.12 | 5.4 |
| Bulk mass ($10^{10}$ kg) | 0.90 | 0.58 | 1.5 |
| Mean eruption rate ($m^3$ $s^{-1}$) | 2.2 | 1.4 | 1.8 |
| Mean eruption rate ($10^3$ kg $s^{-1}$) | 6.1 | 3.8 | 5.0 |
| *Volatile Budget*[f] | | | |
| $H_2O$ ($10^8$ kg) | 2.7 | 1.8 | 4.5 |
| $CO_2$ ($10^8$ kg) | 1.4 | 0.8 | 2.2 |
| $SO_2$ ($10^8$ kg) | 0.6 | 0.4 | 1.0 |
| HCl ($10^8$ kg) | 0.08 | 0.04 | 0.12 |
| Bulk volatiles ($10^8$ kg) | 4.8 | 3.0 | 7.8 |

[a]Data from *Bottari et al.* [1975].
[b]This work.
[c]Computed from a 80% build up of Mount De Fiore pyroclastic cones during the first 3 days of each eruptive phase (see text) and the volumes of lava flows emitted in this interval [*Bottari et al.*, 1975].
[d]Explosivity index, volume of pyroclastites/total volume of pyroclastites plus lava flows.
[e]DRE, dense rock equivalent magma quantities computed after correction for a mean vesicularity of 20% and 50% in lava flows and pyroclastites, respectively, and using the measured density of 2760 kg $m^{-3}$ for water-free Etnean glass at ambient temperature.
[f]Volatile budget derived from the bulk amounts of dense erupted magma and from the initial and residual abundances of volatile species in the melt (see section 5.4).

(3.4 $m^3$ $s^{-1}$ or 2.2 $m^3$ $s^{-1}$ DRE) as the second phase (explosivity index of 0.29 and 1.9 $m^3$ $s^{-1}$ or 1.4 $m^3$ $s^{-1}$ DRE; Table 1). Finally, the prevalent (~80%) build up of DFI and DFII pyroclastic cones during the first 3 days of each eruptive phase [*Tazieff*, 1974; *Bottari et al.*, 1975; *Tanguy and Kieffer*, 1977; R. Romolo, unpublished notes, 1974], together with estimates of contemporaneous lava flow volumes [*Bottari et al.*, 1975], imply a much higher average eruption rate (9.2 and 3.1 $m^3$ $s^{-1}$, respectively) during that initial stage than during subsequent activity.

## 3. Sample Descriptions and Analytical Procedures

[18] Our study of the 1974 eruption products pertains to various samples of lava flows, lava bombs, scoria and crystal-rich lapilli from both DFI and DFII eruptive phases. Most of the samples selected for bulk rock analysis of major and trace elements derive from lava flows (14 samples) collected during the course of the eruption, and from the summit crater activity before (13 January, a lava bomb) and after (18 October, a lava flow) the eruption. These samples, collected by R. Romano, are available in the archives of Istituto Nazionale di Geofisica e Vulcanologia (INGV), in Catania. For melt inclusion studies we additionally collected air-quenched scoria and lapilli from Mount De Fiore I and II cones. For a comparison, we also report new analyses of bulk rocks and olivine-hosted melt inclusions in explosive products from the 1763 La Montagnola DDF flank eruption, collected by *Miraglia* [2002].

[19] The major and trace element contents of bulk rocks were measured using Inductively Coupled Plasma Optical Emission Spectroscopy (ICP-OES) and Inductively Coupled Plasma–Mass Spectrometry (ICP-MS), respectively [*Carignan et al.*, 2001], at the Centre de Recherches Pétrographiques et Géochimiques (SARM) in Nancy (France). Analytical uncertainty ($1\sigma$) is <1% for $SiO_2$ and $Al_2O_3$, <2% for $Fe_2O_3$, MgO, CaO, $Na_2O$, $K_2O$, <5% for MnO, and $TiO_2$ and 5–10% for $P_2O_5$, and <5% for all trace elements except U (<8%).

[20] Minerals and matrix glass compositions were measured at INGV-Catania with a LEO-1430 scanning electron microscope equipped with an Oxford EDS microanalytical system. Routine analytical conditions include acceleration tension of 20 keV, probe current of 1.2 nA, and XPP data reduction. To minimize alkali loss during analysis, a square raster of 10 × 10 $\mu$m has been used. The accuracy of our measurements was checked through replicate analyses of different glass and mineral standards (VG-2 Glass USNM 111240, Chromium augite NMNH 164905, Olivine San Carlos USNM 11131/444, Labradorite USNM115900, Hornblende Kakanui USNM143965, apatite Durango USNM104021 and Chromite USNM117075 [see *Jarosewich et al.*, 1980]). The relative errors ($1\sigma$) are <1% for $SiO_2$, $Al_2O_3$ and FeO, <0.5% for MgO and CaO and between 2 and 3% for $TiO_2$, MnO, $Na_2O$, $K_2O$ and $P_2O_5$ [*Miraglia*, 2006].

[21] Melt inclusions and glass embayments in olivine crystals were analyzed for their chemical composition and S-Cl content using a SX50 CAMECA electron microprobe (Service Camparis, Jussieu, France). Major elements were measured with a 10 nA beam current, 10 $\mu$m spot size, and a counting time of 10 to 25 s. Sulfur, chlorine and phosphorus were determined with a 30 nA beam current, a 15 $\mu$m spot size, and using 200 s counting time. S, Cl, P and carbon (see below) analyses were calibrated against internal reference glasses.

[22] Dissolved carbon in the same melt inclusions was analyzed with the Pierre Sue Laboratory nuclear microprobe (Saclay), using the $^{12}C(d, p)^{13}C$ nuclear reaction (see *Spilliaert et al.* [2006] for details). The samples were irradiated with deuterons at 1.45 MeV incident energy and an integrated charge of 1.5$\mu$C, implying a minimum detection limit of 20 ppm C (i.e., ~75 ppm $CO_2$).

[23] The water content of the inclusions was measured with a CAMECA IMS3f ion microprobe in Max-Planck-Institut fuer Chemie (Mainz, Germany). All measurements were made using an $O^-$ primary beam, 10 nA beam current, 15–20 $\mu$m beam size and $^{30}Si$ as internal standard [*Sobolev and Chaussidon*, 1996]. For calibration, we used synthetic glass standards equivalent in composition to Etna lava and containing 1.19, 1.47, 3.04 and 3.60 wt % $H_2O$ (B. Scaillet, Institut des Sciences de la Terre d'Orléans, France). These same standards were used for measuring the volatile content of olivine-hosted melt inclusions from both the 1763 La Montagnola, 2001 and 2002–2003 flank eruptions of

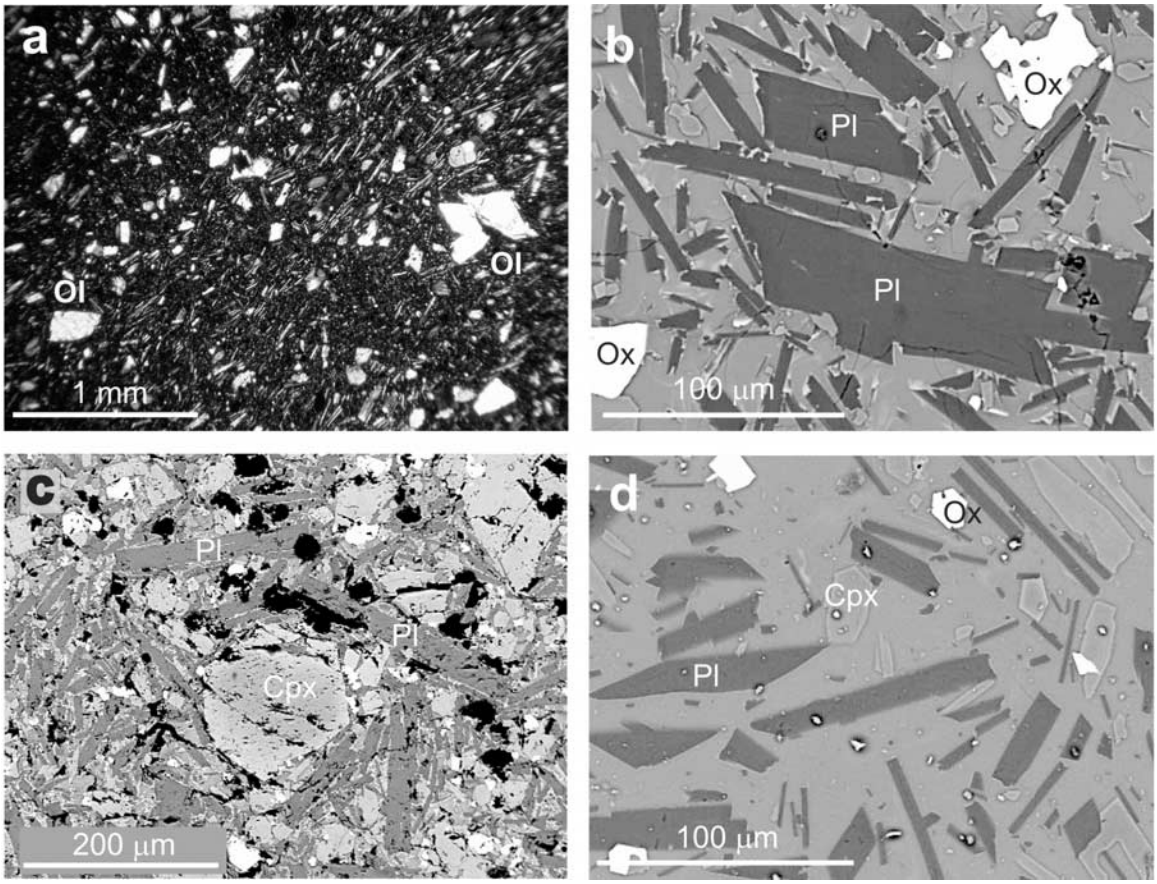


**Figure 3.** Textures of products from the 1974 flank eruption. (a) Lava flow (sample 090274FLA) erupted from DFI scoria cone with scarce phenocrysts of olivine (crossed polarized light). Ol, olivine. (b) Backscattered image of the plagioclase-bearing glassy matrix in a quenched scoria (sample 010274FLA_C) erupted on 1 February from DFI cone. Pl, plagioclase; Ox, oxide. (c) Backscattered image of the typical microlite-rich groundmass of a lava flow (sample 230374) erupted on 23 March from DFII cone. Cpx, clinopyroxene. (d) Backscattered groundmass texture of a lapillus erupted during lava fountaining activity on 27 October 2002. Abbreviations are as in Figures 3b and 3c.

Etna, which then permits direct intercomparison of the corresponding results.

## 4. Petrography, Mineralogy, and Geochemistry of the 1974 Products

### 4.1. Petrography and Bulk Rock Compositions

[24] Bulk rock samples from the 1974 flank eruption maintained a broadly constant petrography and modal mineralogy during both the DFI and DFII eruptive phases. They contain only 1 to 3 vol % phenocrysts (Figure 3a) of olivine, subordinate clinopyroxene, rarer titanomagnetite, and no plagioclase. These erupted products were thus nearly aphyric and differed markedly from common Etna lavas which usually contain a high proportion of phenocrysts (on average 25 vol %) among which plagioclase is the most abundant mineral phase [*Bottari et al.*, 1975; *Tanguy and Kieffer*, 1977; this work].

[25] The groundmass has either a glassy or a cryptocrystalline texture (Figures 3b and 3c), depending on the cooling history. It is mostly composed of microlites (<200 $\mu$m) of tabular plagioclase, granular sector-zoned pyroxene and fewer olivine and opaque oxides, all of which are embedded in a pale yellow glass or fine-grained matrix. Microlites are less abundant and smaller ($\leq$100 $\mu$m; Figure 3b) in rapidly quenched scoria than in the groundmass of lava flows (up to 200 $\mu$m; Figure 3c) and large lava bombs. Otherwise, our scoria samples from the 1974 eruption contain larger microlites than comparable scoria from 2002–2003 eruption (Figure 3d), implying different conditions of degassing and cooling.

[26] Minerals were analyzed in quenched scoria from the DFI eruptive phase (1 and 16 February) and in both lava bombs and flows from the DFII phase (12, 18, and 23 March). Selected compositions of olivine, clinopyroxene and plagioclase are reported in the auxiliary material (Tables S1, S2, and S3).[1] Olivine phenocrysts (>500 $\mu$m) and microphenocrysts (500–200 $\mu$m) from both eruption phases are homogeneous or weakly normally zoned, with most frequent core compositions $Fo_{80-82}$ (Figure 4a) and rims from $Fo_{82}$ to $Fo_{74}$ (Figure 4b). Olivine microlites (200–50 $\mu$m) in the groundmass display a slightly larger compositional range from $Fo_{82}$ to $Fo_{72}$ (Figure 4c). In all products clinopyroxenes are

[1] Auxiliary materials are available in the HTML. doi:10.1029/2008JB006013.

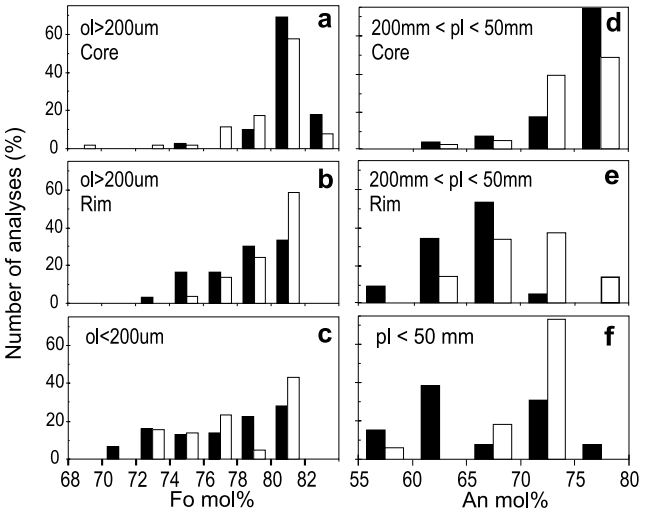


**Figure 4.** Distribution of olivine and plagioclase compositions. Forsterite (Fo mol %) content of the (a) cores and (b) rims of olivine phenocrysts and microphenocrysts (>200 $\mu$m) and (c) of microlites (<200 $\mu$m). Anorthite (An mol %) content of (d) cores and (e) rims of the plagioclase microlites (200–50 $\mu$m) and (f) of the smallest microlites (<50 $\mu$m) in the groundmass. Black and white bars refer to scoria (samples 010274FLA_C and 160274FLA) from the DFI eruptive phase and to bombs and lava flows from DFII phase (samples 120374, 180374, and 230374), respectively.

500–200 $\mu$m euhedral microphenocrysts ($Wo_{51-44}$, $En_{42-32}$, $Fs_{17-12}$) which contain other minerals (olivine and Ti magnetite) and glass inclusions. Backscattered electron imaging shows their systematic sector zoning [*Downes*, 1974], with sectors enriched in either $TiO_2$ and $Al_2O_3$ or $SiO_2$ and MgO. Finally, plagioclase occurs almost exclusively as microlites ranging in size from <50 to 200 $\mu$m. 80% of these microlites have a core composition varying from $An_{80}$ to $An_{70}$ (Figure 4d), the largest ones displaying a more restricted range ($An_{80-75}$). Their rims, as well as the smallest microlites (<50 $\mu$m), have a wider range in anorthite content ($An_{75-55}$; Figures 4e and 4f).

[27] Table 2 shows the major and trace element compositions of selected bulk rocks from both the 1974 flank eruption, 1974 summit activity, and 1763 DDF eruption. Further analyses are given in the auxiliary material (Table S4).

[28] The products erupted during the two phases of the 1974 flank event display very limited variations of both major and most trace elements (Figures 5 and 6), within the limits of analytical uncertainty. Such a chemical homogeneity, especially illustrated by their constant Rb/Nb and Rb/Th ratios (Figures 6e and 6f), points to their derivation from the same magma batch at depth. Figure 5 shows that the 1974 DDF eruption products fall within the compositional domain of potassic trachybasalts [*Le Maitre*, 2002], typical of post-1970 Etna lavas. They closely resemble trachybasalts from the 2001–2003 DDF eruptions [*Clocchiatti et al.*, 2004; *Métrich et al.*, 2004; *Spilliaert et al.*, 2006; *Viccaro et al.*, 2006; *Corsaro et al.*, 2007, also unpublished data, 2004] for both major and trace elements (e.g., Mg # = 0.51–0.52 and Th ~7 ppm, Figures 6a–6d). In contrast, they markedly differ from the 1763 DDF products in having a higher $K_2O$ content (Figure 6b) and higher Rb/Nb and Rb/Th ratios (Figures 6e and 6f). Following the classical terminology used in literature for pre-1970s Etna lavas, these 1763 products were termed hawaiites. However, because Etnean trachybasalts and hawaiites essentially differ by their $K_2O$ content, here we simply refer them as to K-poor and K-rich trachybasalts, respectively (Figure 5).

### 4.2. Comparison With Bulk Products From 1974 Summit Crater Activity

[29] The lava bomb and lava flow recovered from the 1974 summit crater activity sharply differ, both in their mineralogy and geochemistry, from the 1974 flank eruption products (Table 2). First, these summit samples contain 25–30 vol % of phenocrysts, among which idiomorphic plagioclase prevails (15–20 vol %), followed by euhedral clinopyroxene (10–15 vol %), olivine (1–5% vol %) and rare opaque oxides. Microlites in their groundmass show the same paragenesis. These samples are also more evolved chemically, as evidenced by their lower $CaO/Al_2O_3$ ratio, Mg # and Ni content, while higher Th, La, Nb contents (Figures 6c and 6d). Altogether, these features are typical of lavas erupted from the central volcano conduits. Moreover,

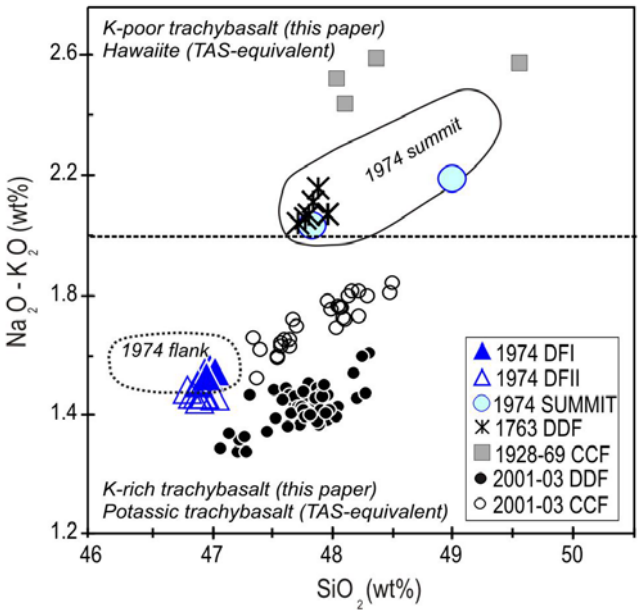


**Figure 5.** Chemical classification of 1974 flank and summit products using subdivision of TAS (total alkali-silica diagram [*Le Maitre*, 2002]). In the text we prefer using the terms "K-poor trachybasalt" and "K-rich trachybasalt," instead of the "hawaiite" and "potassic trachybasalt" TAS nomenclature [*Le Maitre*, 2002]. Analyses of 2001–2003 DDF and CCF eruptions [*Clocchiatti et al.*, 2004; *Métrich et al.*, 2004; *Spilliaert et al.*, 2006; *Corsaro et al.*, 2007, also unpublished data, 2004], 1928–1969 CCF [*Joron and Treuil*, 1984], and 1763 DDF are plotted for comparison. Other published data for products from the 1974 flank eruption (dotted line) and the 1974 summit activity (continuous line) are from *Bottari et al.* [1975], *Tanguy and Kieffer* [1977], *Tanguy* [1980], and *Armienti et al.* [1988].

**Table 2.** Selected Bulk Rock and Glass Compositions of Products Erupted During the 1974 DDF Flank Eruption, the 1974 Summit Crater Activity and the 1763 La Montagnola DDF Flank Eruption[a]

| | 1974 Flank Eruption (DFI Phase) | | | | | 1974 Flank Eruption (DFII Phase) | | | | | 1974 Summit Craters | | 1763 Eruption | | |
|---|---|---|---|---|---|---|---|---|---|---|---|---|---|---|---|
| | Bulk Rock | | | Sideromelane Glassy Matrices | | Bulk Rock | | | Glass Tachylite-Type Matrices | | Bulk Rock | | | | |
| | 1 Feb | 10 Feb | 16 Feb | 1 Feb | 16 Feb | 12 Mar | 18 Mar | 23 Mar | 12 Mar | 23 Mar | 13 Jan | 18 Oct | Bulk Rock | | |
| Sample | 010274FLA_C | 100274FLA | 160274FLA | 010274 | FLA_C | 160274FLA | 120374FLA_A | 180374FLA | 230374FLA | 120374FLA_A | 230374FLA | 130174SUM | 181074SUM | LYMC8 | LYMC17 | LYMC20 |
| Number of analyses | | | | 26 | 14 | | | | 3 | 10 | | | | | |
| Type | scoria | lava flow | scoria | scoria | scoria | bomb | bomb | lava flow | bomb | lava flow | bomb | lava flow | lava flow | lava flow | lava flow |
| $SiO_2$ | 46.44 | 46.26 | 46.41 | 49.15 (0.26) | 49.51 (0.13) | 46.49 | 46.13 | 46.98 | 52.66 (0.96) | 52.76 (1.32) | 47.01 | 48.27 | 46.85 | 47.18 | 47.75 |
| $TiO_2$ | 1.76 | 1.76 | 1.76 | 2.06 (0.09) | 2.03 (0.06) | 1.78 | 1.76 | 1.80 | 1.43 (0.18) | 1.64 (0.29) | 1.73 | 1.64 | 1.60 | 1.62 | 1.63 |
| $Al_2O_3$ | 16.55 | 16.45 | 16.44 | 16.19 (0.24) | 16.26 (0.33) | 16.40 | 16.33 | 16.55 | 17.23 (0.73) | 17.62 (1.24) | 17.11 | 17.91 | 16.34 | 16.83 | 16.87 |
| $Fe_2O_3$ | 1.80 | 1.79 | 1.80 | | | 1.80 | 1.79 | 1.82 | | | 1.72 | 1.59 | 1.76 | 1.76 | 1.78 |
| FeO | 8.98 | 8.93 | 9.00 | 11.73 (0.37) | 11.67 (0.24) | 8.97 | 8.95 | 9.11 | 10.37 (1.21) | 9.40 (1.63) | 8.58 | 7.97 | 8.78 | 8.77 | 8.88 |
| MnO | 0.19 | 0.19 | 0.19 | 0.25 (0.07) | 0.24 (0.05) | 0.19 | 0.18 | 0.19 | 0.33 (0.13) | 0.27 (0.09) | 0.18 | 0.18 | 0.18 | 0.18 | 0.18 |
| MgO | 6.17 | 6.20 | 6.28 | 2.95 (0.23) | 2.98 (0.17) | 6.35 | 6.28 | 6.29 | 1.27 (0.10) | 1.41 (0.33) | 5.38 | 4.48 | 6.41 | 6.19 | 6.29 |
| CaO | 11.11 | 11.28 | 11.18 | 7.50 (0.28) | 7.75 (0.23) | 11.27 | 11.22 | 11.39 | 3.86 (0.46) | 3.23 (0.67) | 10.47 | 9.73 | 10.94 | 10.92 | 10.93 |
| $Na_2O$ | 3.43 | 3.40 | 3.40 | 4.53 (0.22) | 4.35 (0.21) | 3.37 | 3.35 | 3.36 | 5.28 (0.47) | 5.90 (0.37) | 3.78 | 4.14 | 3.36 | 3.41 | 3.40 |
| $K_2O$ | 1.89 | 1.90 | 1.88 | 4.69 (0.12) | 4.21 (0.12) | 1.92 | 1.90 | 1.89 | 6.32 (0.18) | 6.74 (0.53) | 1.78 | 1.98 | 1.34 | 1.34 | 1.35 |
| $P_2O_5$ | 0.54 | 0.54 | 0.54 | 0.95 (0.07) | 1.00 (0.07) | 0.53 | 0.53 | 0.54 | 1.26 (0.08) | 1.02 (0.13) | 0.57 | 0.63 | 0.49 | 0.51 | 0.49 |
| LOI[b] | 0.75 | 0.78 | 0.73 | | | 0.73 | 0.84 | 0.93 | | | 0.73 | 0.65 | 0.88 | 0.80 | 1.04 |
| Total | 99.60 | 99.46 | 99.60 | 100.00 | 100.00 | 99.79 | 99.25 | 100.84 | 100.00 | 100.00 | 99.01 | 99.60 | 98.92 | 99.51 | 100.60 |
| Mg #[c] | 0.51 | 0.51 | 0.51 | | | 0.52 | 0.51 | 0.51 | | | 0.49 | 0.46 | 0.52 | 0.52 | 0.52 |
| $CaO/Al_2O_3$ | 0.67 | 0.69 | 0.68 | 0.46 (0.02) | 0.48 (0.02) | 0.68 | 0.69 | 0.69 | 0.22 (0.03) | 0.19 (0.05) | 0.61 | 0.54 | 0.67 | 0.65 | 0.65 |
| Rb | 44.5 | 43.9 | 43.6 | | | 43.6 | 43.4 | 46.4 | | | 40.9 | 44.0 | 27.5 | 27.53 | 25.43 |
| Cs | 0.90 | 0.86 | 0.87 | | | 0.88 | 0.87 | 0.93 | | | 0.81 | 0.91 | 0.57 | 0.52 | 0.40 |
| Sr | 1242 | 1181 | 1191 | | | 1172 | 1163 | 1247 | | | 1226 | 1232 | 1035 | 1098 | 1059 |
| Ba | 647 | 618 | 630 | | | 615 | 610 | 644 | | | 714 | 784 | 546 | 553 | 561 |
| Ta | 2.5 | 2.4 | 2.4 | | | 2.4 | 2.3 | 2.4 | | | 2.9 | 3.3 | 2.4 | 2.4 | 2.5 |
| Th | 7.4 | 7.3 | 7.3 | | | 7.0 | 7.1 | 7.4 | | | 8.9 | 10.5 | 7.1 | 7.0 | 7.2 |
| U | 2.19 | 2.15 | 2.17 | | | 2.13 | 2.09 | 2.21 | | | 2.54 | 2.96 | 1.97 | 1.98 | 2.01 |
| Zr | 189.4 | 180.9 | 183.9 | | | 180.0 | 177.0 | 189.9 | | | 221.8 | 239.8 | 181.2 | 182.4 | 184.5 |
| Hf | 4.4 | 4.3 | 4.4 | | | 4.3 | 4.3 | 4.4 | | | 4.6 | 5.0 | 4.0 | 3.9 | 4.1 |
| Nb | 42.8 | 40.9 | 41.4 | | | 39.9 | 39.1 | 42.4 | | | 51.6 | 57.9 | 41.1 | 41.7 | 42.3 |
| La | 57.8 | 55.5 | 56.3 | | | 54.7 | 54.2 | 57.7 | | | 65.2 | 72.2 | 52.1 | 52.8 | 54.1 |
| Ce | 111.2 | 102.3 | 104.0 | | | 101.6 | 100.6 | 111.0 | | | 122.9 | 134.4 | 98.8 | 99.7 | 101.7 |
| Nd | 49.2 | 46.6 | 47.4 | | | 46.6 | 46.3 | 48.6 | | | 52.0 | 54.5 | 43.3 | 44.0 | 44.9 |
| Sm | 9.48 | 9.09 | 9.11 | | | 9.05 | 8.96 | 9.64 | | | 9.71 | 9.87 | 8.20 | 8.15 | 8.38 |
| Eu | 2.88 | 2.74 | 2.78 | | | 2.75 | 2.73 | 2.88 | | | 2.94 | 2.88 | 2.47 | 2.50 | 2.50 |
| Tb | 1.03 | 1.01 | 1.02 | | | 1.01 | 1.00 | 1.06 | | | 1.05 | 1.06 | 0.89 | 0.88 | 0.91 |
| Yb | 2.19 | 2.07 | 2.12 | | | 2.08 | 2.09 | 2.16 | | | 2.24 | 2.28 | 1.92 | 1.91 | 1.94 |
| Lu | 0.32 | 0.31 | 0.31 | | | 0.31 | 0.30 | 0.32 | | | 0.33 | 0.35 | 0.29 | 0.29 | 0.30 |
| Y | 26.9 | 25.8 | 26.2 | | | 25.7 | 25.4 | 27.2 | | | 27.6 | 28.0 | 23.1 | 23.5 | 23.8 |
| Ni | 34 | 32 | 34 | | | 33 | 33 | 35 | | | 26 | 19 | 39 | 35 | 35 |
| Cr | 46 | 42 | 44 | | | 46 | 50 | 49 | | | 30 | 17 | 62 | 52 | 55 |
| V | 328 | 325 | 324 | | | 322 | 313 | 343 | | | 307 | 262 | 301 | 306 | 300 |
| Co | 42 | 41 | 42 | | | 41 | 41 | 44 | | | 38 | 33 | 42 | 42 | 41 |
| Cu | 147 | 151 | 142 | | | 139 | 136 | 152 | | | 134 | 137 | 140 | 142 | 94 |

[a]Additional bulk rock compositions for both 1974 and 1763 DDF flank eruptions are available in Table S4 in the auxiliary material. Values in parentheses are standard deviations.
[b]LOI, Loss on ignition.
[c]Mg #, [(Mg/(Mg + $Fe^{2+}$)] moles per 100 assuming $Fe^{3+}/Fe^{2+}$ = 0.2.

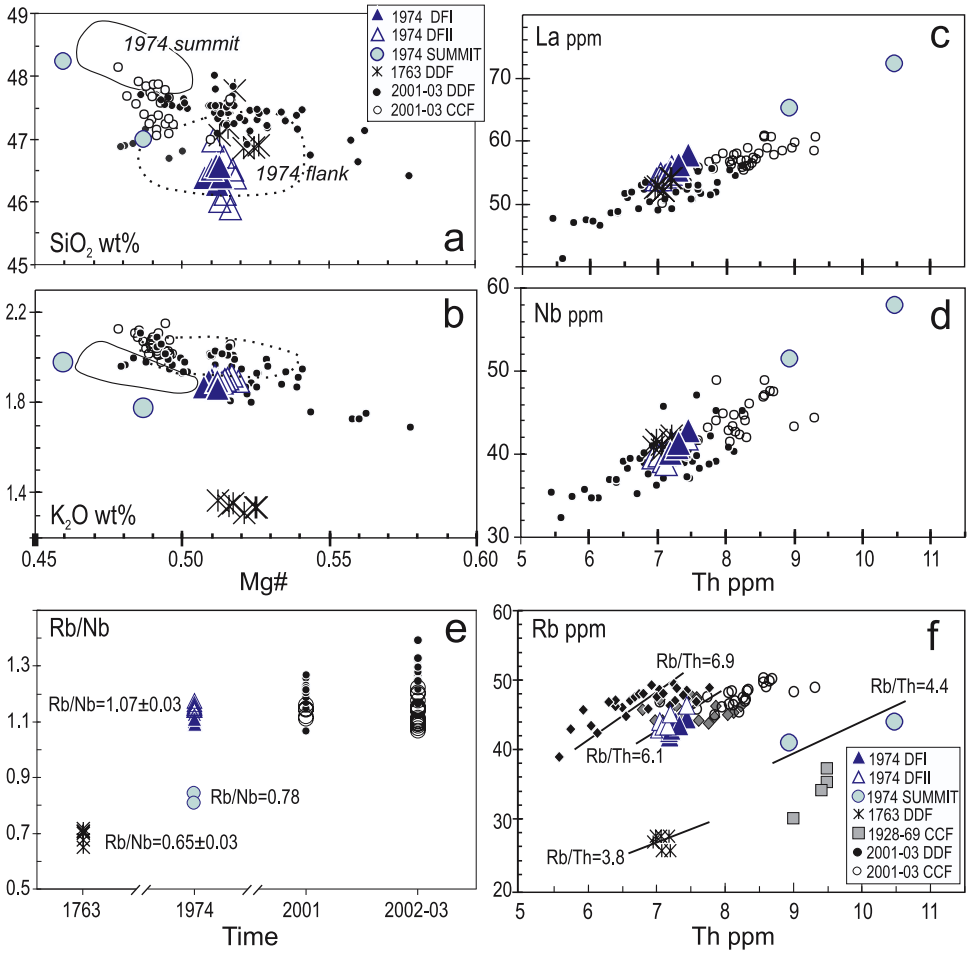


**Figure 6.** Major and trace element compositions of the 1974 flank and summit products. (a and b) Variations of Mg # versus $SiO_2$ and $K_2O$. Mg # = Mg/(Mg + $Fe^{2+}$) moles per 100 assuming $Fe^{3+}/Fe^{2+} = 0.2$. (c, d, f) Variations of La, Nb, and Rb versus Th. (e) Temporal variation of the Rb/Nb ratio [*Clocchiatti et al.*, 2004; *Métrich et al.*, 2004; *Spilliaert et al.*, 2006; *Corsaro et al.*, 2007, also unpublished data, 2004]. The chemistry of 1974 flank trachybasalt is well explained by the mixing between K-rich and K-poor trachybasaltic magmas having a similar degree of evolution (Th = 7 ppm), whose 1763 and 2002–2003 DDF lavas are representative end-members (see text). The 1974 summit products, as well as lavas erupted in 1928–1969 [*Joron and Treuil*, 1984], show a prevalent imprint of 1763-type low-K trachybasalts. Symbols are the same as in Figure 5.

these products plot into the K-poor trachybasalt field (Figure 5) and have Rb/Nb and Rb/Th ratios closer to those of pre-1970s Etna lavas (Figure 6e and 6f). More broadly, they differ from all products emitted by Etna in the post-1974 decades, including the 2001–2003 lavas drained from the central conduits [*Clocchiatti et al.*, 2004; *Métrich et al.*, 2004; *Spilliaert et al.*, 2006; *Corsaro et al.*, 2007, also unpublished data, 2004].

### 4.3. Matrix Glasses

[30] Analyses were performed on glassy (“sideromelane-type”) matrix of rapidly cooled scoria from the DFI eruptive phase and on cryptocrystalline (“tachylite-type”) matrix in bombs and lava samples from the DFII phase (Table 2). DFI glassy matrices (Figure 3b) are homogeneous, with average $CaO/Al_2O_3$ ratios from 0.46 to 0.48. In contrast, tachylitic DFII matrices are richer in microlites (Figure 3c), with residual glasses more evolved ($0.18 < CaO/Al_2O_3 < 0.43$) than in DFI matrices. These features reflect late stage subsurface crystallization, a process already described by *Corsaro and Pompilio* [2004]. Mass balance calculations indicate microlite crystallization of 29% of plagioclase ($An_{65}$) and 9% of clinopyroxene ($Wo_{45}En_{41}Fs_{14}$).

[31] We assessed the eruptive temperatures using the empirical geothermometer of *Pompilio et al.* [1998] for Etnean volcanic glasses. The calculated equilibrium temperature for the glassy matrices is 1075 ± 10°C and agrees with the temperature of 1085°C measured in flowing lava during the eruption [*Tanguy and Kieffer*, 1977]. Such temperatures are quite typical for erupting Etnean trachybasalts [*Pompilio et al.*, 1998]. We infer lower temperatures of 1025 to 1040°C (±10) for the tachylitic products, in agreement with their higher microlite content.

### 4.4. Olivine-Hosted Melt Inclusions

[32] Olivine crystals and their melt inclusions were analyzed in lapilli and scoria from both the 1974 and 1763 DDF eruptions (Table 3). In samples from both eruptions,

**Table 3.** Selected Compositions of Olivine-Hosted Melt Inclusions From the 1974 and 1763 La Montagnola DDF Flank Eruptions[a]

| | 1974 Eruption (DFI Phase) | | | | | | | 1974 Eruption (DFII Phase) | | | | 1763 Eruption | | | | | |
|---|---|---|---|---|---|---|---|---|---|---|---|---|---|---|---|---|---|
| Sample | 2–1 | 3 | 6b | 1 | 33 | 34b | 26 | 52a | 52b | 58a | 56 | 7 | 14 | 33c | 37 | 36 | 31 |
| Fo[b] (mol %) | 79.8 | 81.5 | 80.0 | 78.7 | 81.0 | 81.6 | 80.0 | 81.9 | 80.8 | 81.1 | 80.6 | 80.4 | 81.1 | 80.4 | 80.9 | 80.4 | 82.2 |
| PEC[c] (%) | 0.00 | 0.03 | 0.00 | 0.01 | 0.04 | 0.02 | 0.06 | 0.00 | 0.00 | 0.00 | 0.06 | 0.000 | 0.000 | 0.025 | 0 | 0.01 | 0.005 |
| $SiO_2$[d] | 44.14 | 42.87 | 44.99 | 44.05 | 43.10 | 44.22 | 48.11 | 44.83 | 43.77 | 44.23 | 48.61 | 44.75 | 45.29 | 44.18 | 46.01 | 45.38 | 44.60 |
| $TiO_2$ | 1.64 | 1.58 | 1.71 | 1.75 | 1.78 | 1.69 | 1.86 | 1.64 | 1.63 | 1.67 | 1.53 | 1.65 | 1.63 | 1.58 | 1.62 | 1.59 | 1.62 |
| $Al_2O_3$ | 15.99 | 15.38 | 16.04 | 15.33 | 16.20 | 15.37 | 15.59 | 15.58 | 15.60 | 15.51 | 17.46 | 16.12 | 16.77 | 16.77 | 16.85 | 15.75 | 16.38 |
| $FeO_{TOT}$ | 10.86 | 11.94 | 10.31 | 11.71 | 11.35 | 10.74 | 11.09 | 10.47 | 10.70 | 10.97 | 10.13 | 9.75 | 10.09 | 10.53 | 9.50 | 10.84 | 9.52 |
| MnO | 0.12 | 0.16 | 0.21 | 0.19 | 0.15 | 0.23 | 0.16 | 0.13 | 0.26 | 0.17 | 0.20 | 0.18 | 0.14 | 0.20 | 0.15 | 0.20 | 0.17 |
| MgO | 6.04 | 6.94 | 5.98 | 5.68 | 6.46 | 6.32 | 5.99 | 6.26 | 6.03 | 6.13 | 5.61 | 5.75 | 5.81 | 5.84 | 5.80 | 5.96 | 5.91 |
| CaO | 9.95 | 10.74 | 10.55 | 9.96 | 10.89 | 10.54 | 8.29 | 10.30 | 10.42 | 10.51 | 8.91 | 10.70 | 11.12 | 11.21 | 10.91 | 11.22 | 11.46 |
| $Na_2O$ | 3.45 | 3.09 | 3.03 | 3.19 | 3.21 | 3.09 | 4.45 | 3.21 | 3.37 | 3.09 | 4.15 | 3.15 | 3.22 | 3.29 | 3.24 | 3.13 | 3.15 |
| $K_2O$ | 1.46 | 1.81 | 1.89 | 1.49 | 1.93 | 1.73 | 2.82 | 1.89 | 1.92 | 1.89 | 2.50 | 1.05 | 1.04 | 1.00 | 1.13 | 1.10 | 1.13 |
| $P_2O_5$ | 0.50 | 0.55 | 0.56 | 0.52 | 0.55 | 0.56 | 0.80 | 0.54 | 0.56 | 0.54 | 0.80 | 0.40 | 0.45 | 0.35 | 0.44 | 0.48 | 0.45 |
| S | 0.386 | 0.362 | 0.335 | 0.320 | 0.345 | 0.301 | 0.012 | 0.345 | 0.377 | 0.353 | 0.010 | 0.288 | 0.285 | 0.251 | 0.338 | 0.227 | 0.244 |
| Cl | 0.214 | 0.196 | 0.186 | 0.217 | 0.204 | 0.195 | 0.235 | 0.184 | 0.197 | 0.194 | 0.250 | 0.252 | 0.196 | 0.190 | 0.240 | 0.279 | 0.284 |
| $H_2O$ | 3.5 | 2.6 | 2.7 | 2.8 | 1.7 | 3.0 | 0.3 | 3.5 | 2.9 | 3.0 | 0.3 | 3.0 | 2.8 | 2.3 | 3.2 | 2.6 | ND |
| $CO_2$ | ND | 0.313 | 0.039 | 0.156 | 0.074 | 0.051 | ND | 0.084 | 0.204 | 0.103 | ND | 0.1960 | 0.1632 | 0.129 | 0.123 | 0.116 | ND |
| Total | 98.24 | 98.57 | 98.54 | 97.32 | 97.98 | 97.99 | 99.73 | 98.95 | 97.90 | 98.32 | 100.42 | 97.25 | 99.00 | 97.81 | 99.54 | 98.88 | 94.92 |
| $CaO/Al_2O_3$ | 0.62 | 0.70 | 0.66 | 0.65 | 0.67 | 0.69 | 0.53 | 0.66 | 0.67 | 0.68 | 0.51 | 0.66 | 0.66 | 0.67 | 0.65 | 0.71 | 0.70 |
| $K_2O/Na_2O$ | 0.42 | 0.59 | 0.62 | 0.47 | 0.60 | 0.56 | 0.63 | 0.59 | 0.57 | 0.61 | 0.60 | 0.33 | 0.32 | 0.30 | 0.35 | 0.35 | 0.36 |
| S/Cl | 1.80 | 1.85 | 1.81 | 1.5 | 1.7 | 1.5 | 0.05 | 1.9 | 1.9 | 1.8 | 0.04 | 1.14 | 1.45 | 1.33 | 1.41 | 0.81 | 0.86 |
| Pressure[e] | ND | 392 | 126 | 257 | 116 | 159 | ND | 228 | 310 | 215 | ND | 309 | 257 | 219 | 248 | 205 | ND |
| Pressure[f] | ND | 419 | 117 | 290 | 156 | 148 | ND | 213 | 328 | 222 | ND | 295 | 254 | 207 | 221 | 215 | ND |

[a]The compositions are corrected for postentrapment olivine crystallization (PEC%); ND, not determined.
[b]Forsterite content (mol %) of olivine [100 × Mg/(Mg + Fe)].
[c]Percentage of postentrapment olivine crystallization using $K_D = [(FeO/MgO)_{ol}/(FeO/MgO)_{melt}]$ of 0.29 to 0.30 for equilibrium partitioning of FeO and MgO between olivine and liquid in Etna basalt following *Spilliaert et al.* [2006].
[d]The concentrations of major elements, S, Cl, $H_2O$ and $CO_2$ are in wt %.
[e]Pressure in MPa calculated from the dissolved contents of water and $CO_2$ using VolatileCalc [*Newman and Lowenstern*, 2002].
[f]Pressure in MPa calculated from the dissolved contents of water and $CO_2$ using the model of *Papale et al.* [2006], assuming 1140°C and $fO_2$ close to NNO.

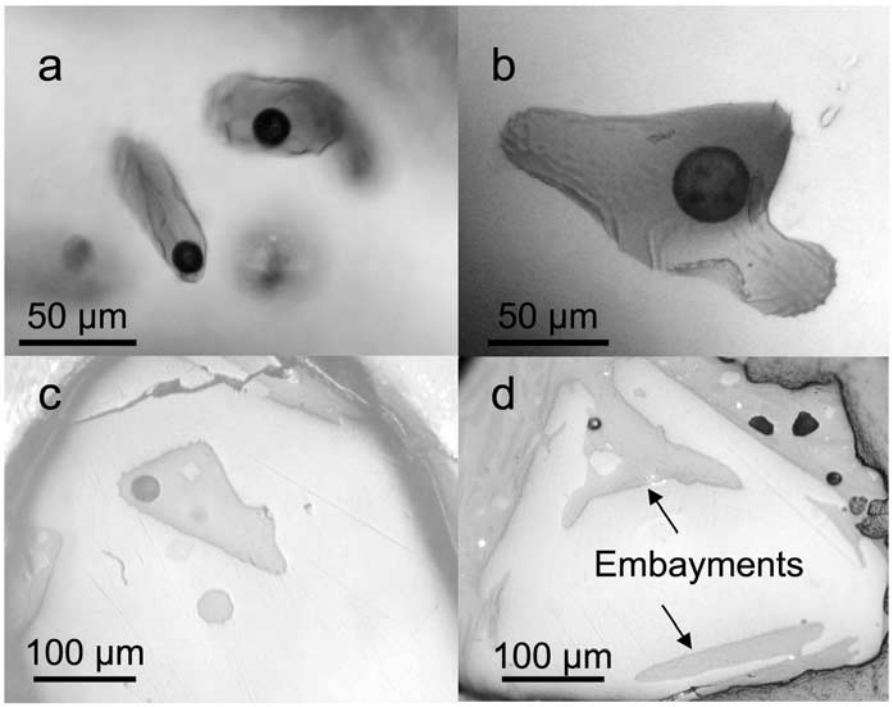


**Figure 7.** Photos of (a–c) olivine-hosted melt inclusions in scoria from Mount De Fiore pyroclastic cones (samples MDF 12 and MDF 13) and (d) of a typical glass embayment formed during rapid olivine growth.

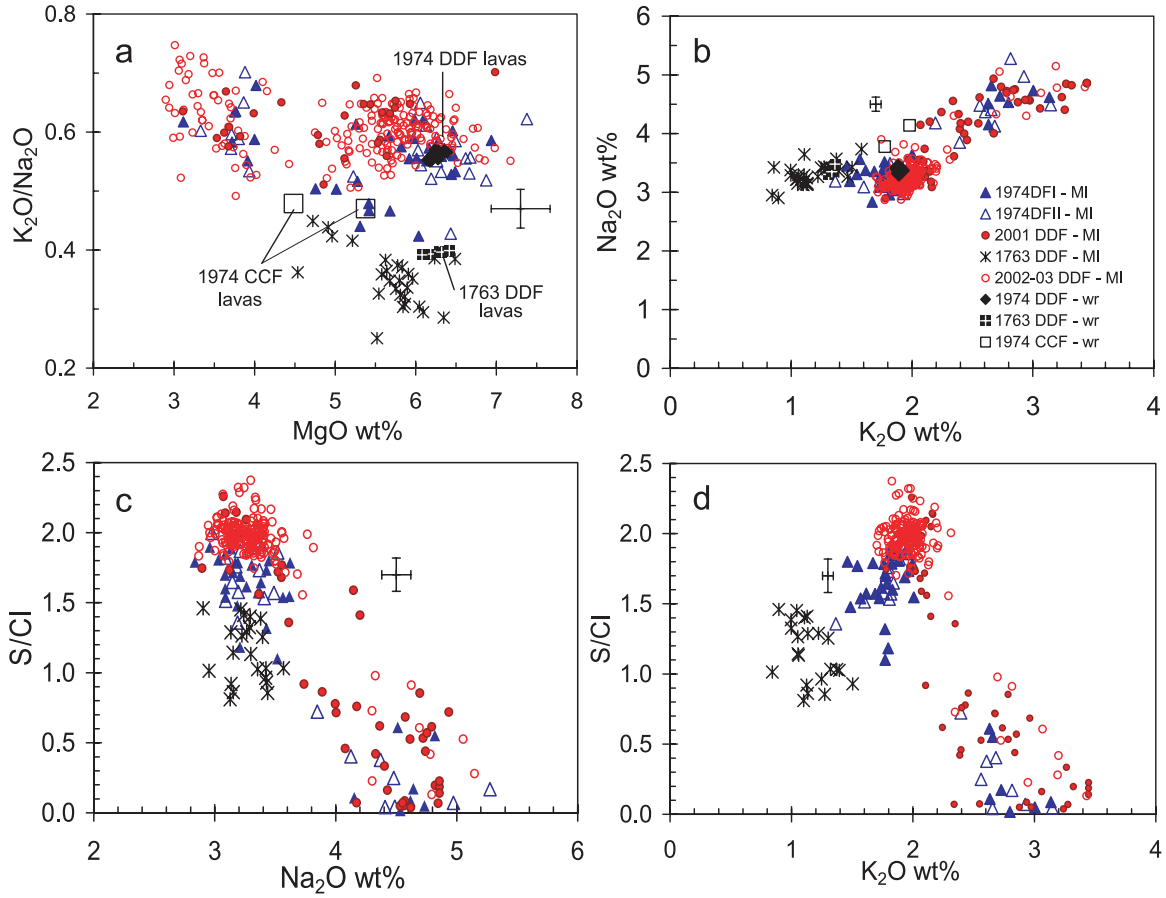


**Figure 8.** Variations (a, b) of alkali concentrations and (c, d) of the $K_2O/Na_2O$ and S/Cl ratios in olivine-hosted melt inclusions and glass embayments from the 1974 and 1763 DDF scoriae. Data for melt inclusions in explosive products from the 2001 and 2002–2003 DDF eruptions [*Métrich et al.*, 2004; *Spilliaert et al.*, 2006] are reported for comparison. Additional data for melt inclusions from 2002 to 2003 DDF flank eruptions are available in Table S5 in the auxiliary material. Note that the compositions of most primitive melt inclusions trapped in the 1974 olivines are similar to those of the bulk lavas.

olivines have the typical skeletal morphology of fast growing microphenocrysts. They are compositionally homogeneous ($Fo_{82-80}$), with thin rims whose forsterite content is lower by only ~1% (as described in section 4.1). Owing to the nearly aphyric nature of both 1974 and 1763 magmas and the small size of their olivines, we could find only rare crystals containing melt/glass inclusions large enough to be analyzed.

[33] Melt inclusions entrapped in 1974 olivines have variable sizes and morphologies. They range from scarce small (30–50 $\mu$m) inclusions with ovoid shape (Figure 7a) to prevalent, larger (50–100 $\mu$m) ones with curvilinear form (Figures 7b and 7c) which are typical for highly dynamic melt entrapment. Most inclusions have a trachybasaltic composition and display $CaO/Al_2O_3$ (0.70–0.66) and $K_2O/Na_2O$ (0.57 ± 0.3) ratios that closely match those of the whole rocks (Figures 8a and 8b). This demonstrates their cogenetic relationship with and representativeness of the bulk magma.

[34] As a whole, the melt inclusions are rich in volatiles (between 4 and 2.8 wt %; Table 3). They contain high amounts of $H_2O$ (from 3.5 to 1.9 wt %), sulfur (3620–3000 wt ppm) and chlorine (2200–1840 wt ppm), while more variable amount of $CO_2$ (from 3100 to 400 wt ppm). Most of them display a constant S/Cl ratio of 1.7 ± 0.2 (Figures 8c and 8d), except for a group of inclusions from the first eruptive phase (DFI) whose S/Cl and $K_2O/Na_2O$ ratios are intermediate between those typical for the 1763 (K-poor) and 2001–2003 (K-rich) Etnean trachybasalts (Figure 8). This suggests a variable mixing between these two end-members. We find that the 1974 eruption products (1) display similar $H_2O$ and $CO_2$ initial contents and ranges as the 2001–2003 K-rich trachybasalts (Figures 9a and 9b) and (2) do not differ in their initial water content (~3–3.5 wt %) from the most primitive samples of 1763 K-poor trachybasalts (Table 3). In other words, these new results indicate a decoupling between the initial water content of Etna magmas and their recent increase in potassium and other alkalis. Otherwise, preferential degassing of poorly soluble carbon dioxide during magma ascent is demonstrated by the almost vertical drop of $CO_2$ at constant $K_2O$ content (Figure 9b), and by the fact that inclusions that are the most depleted in $CO_2$ (0.04–0.05 wt %) could preserve quite a high dissolved amount of water (from 2.7 to 1.7 wt %).

[35] Finally, glass embayments in the 1974 olivines (Figure 7d) provide a record of the magma evolution and degassing during late stage decompression. Compared to melt inclusions, these glasses are systematically more

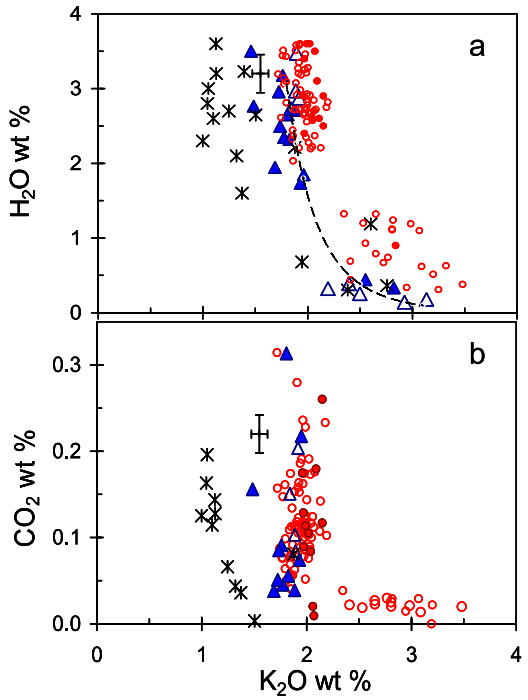


**Figure 9.** Evolutions of (a) $H_2O$ and (b) $CO_2$ dissolved in olivine-hosted melt inclusions as a function of their $K_2O$ content. Same symbols as in Figure 8.

evolved (MgO < 4wt %; Figure 8a) and depleted in both sulfur (<50 wt ppm, S/Cl < 1; Figure 8d) and water (<0.5 wt %; Figure 9a). Only their Cl content (from 2300 to 2500 wt ppm) is preserved or enhanced, evidencing a greater solubility of chlorine compared to $H_2O$ and S.

## 5. Discussion

### 5.1. Previous Interpretations of the 1974 Flank Eruption

[36] Scientists who studied the 1974 eruption [*Guest et al.*, 1974; *Bottari et al.*, 1975; *Guerra et al.*, 1976; *Tanguy and Kieffer*, 1977] published contradictory interpretations of its source depth and origin which, as shown below, can be revisited on the basis of our present results.

[37] As already emphasized, the aphyric nature and peculiar mineralogical features of the 1974 trachybasaltic magma clearly exclude its possible derivation [*Guerra et al.*, 1976] from the central volcano conduits. The same argument holds against the hypothesis by *Bottari et al.* [1975] that it might have derived from a stored residual magma batch of the February–March 1763 eruption that had built the nearby Mount Nuovo and Mount Mezza Luna cones (Figure 1a): this event actually produced a plagioclase-rich and K-poor magma [*Tanguy and Kieffer*, 1977], typical for pre-1970s Etna magmas drained out from the volcano conduits (CCF flank eruption). More generally, the suggestion of a shallow preeruptive storage of the 1974 magma beneath the western flank of Etna, advocated from the high viscosity and high microlite content of the emitted lava flows [*Guest et al.* 1974; *Bottari et al.*, 1975], is poorly compatible with the aphyric character of the magma and other lines of evidence: (1) the small size and the morphology of its olivine crystals, typical for a highly dynamic growth, (2) the lack of euhedral olivine crystals that could have formed during previous ponding; (3) the lack of plagioclase phenocrysts and the high explosivity of the eruption, which both attest of a high decompression rate of the $H_2O$-rich bubbly magma until close to the surface; and (4) our finding of fresh (unmetamorphosed) siliceous sedimentary xenoliths in the eruption products, which indicates only brief mechanical interactions of the magma with the Numidian Flysch units constituting the upper 2–3 km of Mount Etna sedimentary basement [*Lentini*, 1982; *Chiarabba et al.*, 2000]. Altogether, these features rather point to a deep and highly dynamic ascent of the 1974 trachybasalt, with negligible preeruptive ponding in the shallow crust which, otherwise, would have promoted its gradual cooling, degassing and crystallization.

[38] *Tanguy and Kieffer* [1977] actually proposed a direct ascent of the 1974 magma, from mantle depths of 20–30 km, considering its relatively primitive composition and peculiar mineralogy. However, the erupted trachybasalt has much lower MgO and CaO contents than expected for primary Etna magmas [*Armienti et al.*, 1988], best represented by the very rare picritic basalt that could reach the surface during Etna's history (i.e., 3930 years B.P. eruption [*Kamenetsky et al.*, 2007]). Its bulk composition and the moderate forsterite content ($Fo_{82}$) of its Mg-richest olivine crystals rather point to its derivation from a more primitive magma that previously fractionated mafic minerals at depth. Moreover,

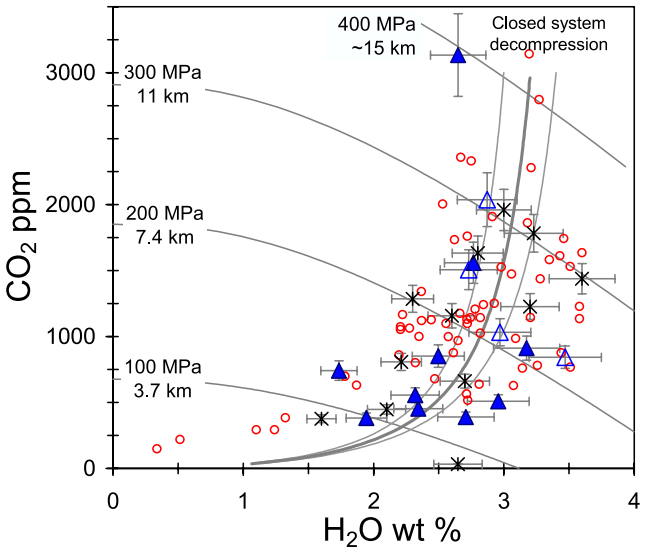


**Figure 10.** Entrapment (total fluid) pressures of olivine hosted melt inclusions in scoria from the 1974 and 1763 DDF eruptions. Total fluid pressures and degassing curves were calculated on the basis of the $H_2O$ and $CO_2$ dissolved contents of melt inclusions, using VolatileCalc [*Newman and Lowenstern*, 2002] and following the same procedure as described by *Spilliaert et al.* [2006]. Data for melt inclusions from the 2001 and 2002–2003 eruptions [*Métrich et al.*, 2004; *Spilliaert et al.*, 2006] are shown for comparison. The computed curves are for closed system decompression of the 1974 trachybasalt containing from 3.0 to 3.4 wt % of $H_2O$ (light gray curves), with a mean at 3.2 wt % (black curve), and coexisting with 1.5 wt % of gas at 300 MPa. The lithostatic depths are indicated in km. Symbols are the same as in Figure 8. See text for discussion.

in the 1974 flank products we found no dense $CO_2$-rich fluid phases, entrapped as either isolated fluid inclusions or in the bubbles of melt inclusions, which could support a direct magma rise from mantle depths. Such deeply derived $CO_2$-rich fluids were only encountered in the tholeiitic and alkaline basalts erupted during the initial (0.3–0.2 Ma) building stage of Mount Etna [*Frezzotti et al.*, 1991] and in primitive olivine of the 7 ka Mount Maletto alkaline basalt [*Kamenetsky and Clocchiatti*, 1996]. Finally, a direct magma rise from 20 to 30 km depths is hardly compatible with the very short interval (6 days) between the precursory earthquakes at such depths (23 km on 24 January [*Bottari et al.*, 1975]) and the eruption outbreak on 30 January.

### 5.2. Source Depth and Conditions of Ascent of the 1974 Trachybasaltic Magma

[39] Our melt inclusion data provide quantitative constraints for the source depths of the 1974 magma. The dissolved $H_2O$ and $CO_2$ contents of olivine-hosted melt inclusions and glass embayments allow us to assess the total fluid pressure ($P_{CO2} + P_{H2O}$) at the time of melt entrapment, assuming volatile saturation. Such a condition is verified at Etna whose alkali magmas originally contain high amounts ($\geq$1.5–2.0 wt %) of carbon dioxide [*Allard et al.*, 1991; *Aiuppa et al.*, 2007] and early coexist with abundant $CO_2$-rich gas [*Métrich et al.*, 2004; *Spilliaert et al.*, 2006]. Total fluid pressures were computed with the VolatileCalc program [*Newman and Lowenstern*, 2002] and for an initial magma temperature of 1140°C [*Métrich et al.*, 2004], taking account of the effect of magma composition on $CO_2$ solubility [*Dixon*, 1997] and hence on calculated equilibrium pressures [*Spilliaert et al.*, 2006].

[40] The values obtained vary from ~400 to 100 MPa (Figure 10) and do not differ significantly from those (Table 3) alternatively computed using the *Papale et al.* [2006] model. They demonstrate polybaric melt entrapment during magma ascent from lithostatic depths of ~15 to 3.7 km, given the average density of lithological units in Etna's crustal basement [*Corsaro and Pompilio*, 2004]. Interestingly, the highest entrapment pressure of 400 MPa, corresponding to ~12 km depth below sea level (bsl), closely matches the focal depths of major earthquakes that marked the early preeruptive seismicity on 21 January 1974 (Figure 1b). Here we simply consider with caution this upper value because it concerns only one inclusion and because $CO_2$ solubility in water-rich basalts is poorly constrained at high pressure [*Spilliaert et al.*, 2006]. At least, our data set shows that the 1974 magma rose from a minimal depth of ~11 km (300 MPa) below Etna's summit, or ~8 km bsl. It is worthy of note that comparable rise depths were inferred for aphyric magmas extruded during the 2001 and 2002–2003 DDF eruptions [*Métrich et al.*, 2004; *Spilliaert et al.*, 2006] and are here indicated by our new results for the 1763 La Montagnola basaltic magma (Figure 10). Such depths approximately correspond to the estimated interface (10 ± 2 km; Figure 1b) between the base of the Hyblean carbonate platform and the lower crystalline crust [*Lentini*, 1982; *Chiarabba et al.*, 2000], where both geophysical data [*Murru et al.*, 1999; *Patanè et al.*, 2002; *Chiarabba et al.*, 2004; *Bonaccorso and Davis*, 2004] and geochemical data [*Métrich et al.*, 2004; *Spilliaert et al.*, 2006] indicate magma storage. We thus infer that the intrusion that fed the 1974 flank eruption likely originated from that intermediate magma storage zone.

[41] The conditions of ascent of the 1974 trachybasaltic magma can be deduced from the overall evolution of dissolved water and carbon dioxide in the melt inclusions with pressure (Figure 10). Taking account of the analytical uncertainties on measured $H_2O$ and $CO_2$ contents, our data for both the DFI and DFII eruptive phases broadly fit with a closed system decompression and degassing of the magma between 10 ± 2 km (400–300 MPa) and ~2 km (100 MPa) depth bsl (given the 1650 m asl elevation of the eruption site). Best data fitting is obtained for a melt initially containing 3.2 ± 0.2 wt % of $H_2O$, 3000–2800 wt ppm of $CO_2$, and coexisting with about 1.5 wt % of exsolved gas at ~400 MPa. The few data points scattered on either side of the mean closed system decompression (CSD) curve are taken to reflect nonequilibrium degassing during fast melt decompression, leading to either $CO_2$ oversaturation or $CO_2$ depletion, in agreement with the peculiar morphology of the inclusions (section 4.4). We could not find any melt inclusion or glass embayment allowing us to track the shallower (<100 MPa) course of the magma. However, lava fountaining and the high eruption rate at the onset of each eruptive phase of the 1974 event (Table 1) suggest that closed system ascent conditions could have been preserved until very close to the surface. This is consistent with the homogeneous $An_{78-75}$ core composition of the largest plagioclase microlites (200 $\mu$m) present in the groundmass of quenched scoria: as shown by experiments on Etna basalt [*Métrich and Rutherford*, 1998], such plagioclase only starts crystallizing when dissolved water is $\leq$1.6 wt %, that is under $P_{H2O} \leq 27$ MPa at 1070°C. These largest microlites thus began to nucleate and grow during magma flow and degassing across the upper kilometre of the feeding intrusion.

[42] Otherwise, several observations evidence that, quite soon after the initial stage of each eruptive phase, gas-melt separation and open degassing developed in the upper portion of the feeding intrusion, while the magma rise speed was probably diminishing. These observations include (1) the rapid transition to and prevalence of Strombolian-style explosive activity, which implies the coalescence and then differential rise of gas slugs that periodically bursted at the vent [e.g., *Jaupart and Vergniolle*, 1989]; (2) the lack of a well-shaped eruption column, as well as the sluggishness and short length of the lava flows [*Guest et al.*, 1974; *Bottari et al.*, 1975; *Tanguy and Kieffer*, 1977], which both indicate extensive outgassing of the magma prior to either fragmentation or flowage at the surface; and (3) the high aspect ratio (Figure 3b) and zoning of the smallest plagioclase microlites (<50 $\mu$m) in quenched scoria, which point to the late nucleation and growth of these microlites during multistage, rather than single-stage melt decompression [*Couch et al.*, 2003].

### 5.3. Triggering Mechanism of the 1974 Dike Intrusion and Flank Eruption

[43] As shown above, the 1974 eruption was likely driven by a magma intrusion that rose from ~10 ± 2 km depth bsl. The spatial and temporal evolution of the precursory seismic crisis provides key insights into the possible triggering mechanism of the intrusion. As argued by *Bottari et al.*

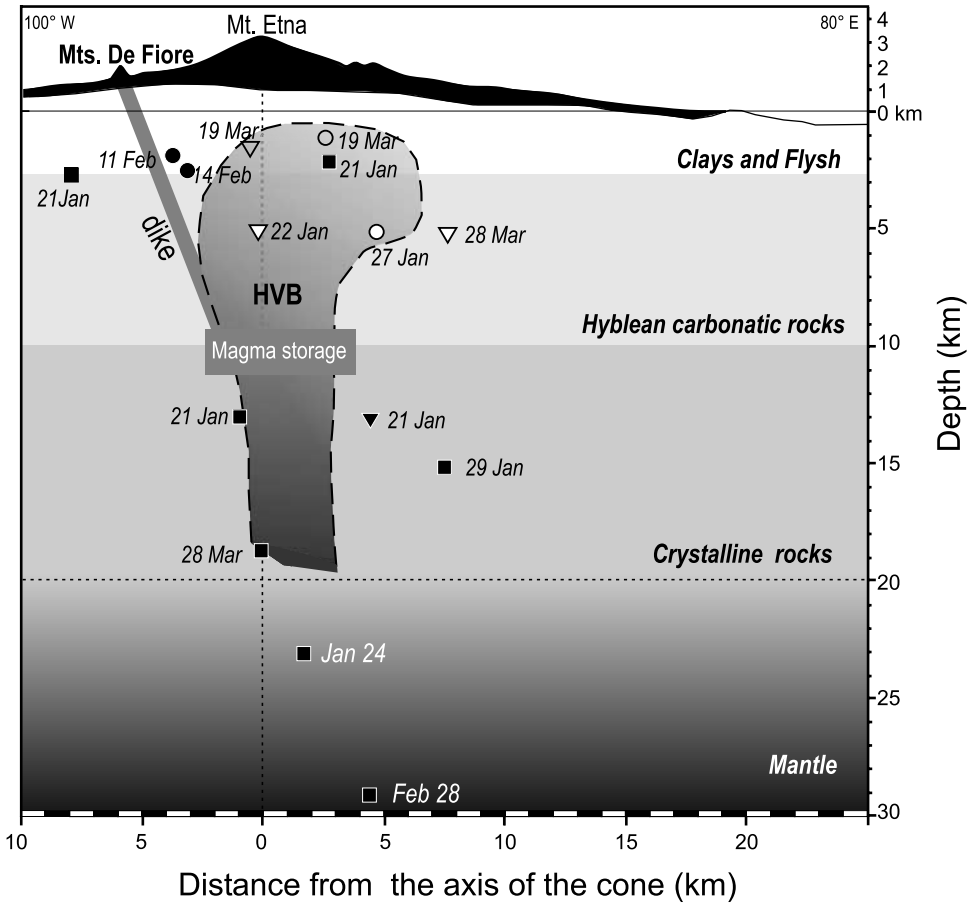


**Figure 11.** Schematic drawing of the dike-forming magma intrusion that fed the 1974 flank eruption, as inferred from seismic data and our melt inclusion results. The intrusion, triggered by tectonic fracturing of Etna's crustal basement, nucleated from a magma storage zone at the base of the Hyblean carbonate platform, where mixing between former K-poor and the new K-rich trachybasalts was occurring at that time. According to the epicentral distribution (Figure 1a) and the focal depths of most energetic earthquakes [*Bottari et al.*, 1975], the dike-like magma intrusion may have propagated along a ENE–WSW 70° inclined plane, on the western border of the high-velocity body (HVB) described by *Chiarabba et al.* [2004]. See Figure 1b for the references to the crustal basement stratigraphy and for the significance of earthquake symbols.

[1975], the high energy (several earthquakes with magnitude $\geq$4) of this preeruptive seismicity, its concentration along a ENE–WSW volcano-tectonic structure of regional direction (Figure 1a), and its rapid deepening during the first hours and days from the upper sedimentary basement down to the local Moho ($\sim$23 km bsl [*Hirn et al.*, 1991; *Chiarabba et al.*, 2000]) strongly suggest its prevalent tectonic origin. In particular, the downward earthquake migration and the short interval between the deepest (23 km) earthquake on 24 January and the eruption outbreak preclude the alternative possibility of a magma input from the base of the crust that would have overpressurized the feeding system and then triggered the intrusion. For instance, the powerful September–October 1989 summit eruption of Etna, that was clearly due to magma input from Moho depths, was anticipated by about 1 year of upward (not downward) migration of earthquake swarms [*Castellano et al.*, 1993]. Rather, the 1974 preeruptive seismic sequence points to a rapid downward fracturing of the crust underlying the whole western half of the volcano that probably depressurized the intermediate feeding system and triggered the propagation of a dike-like intrusion (Figure 11). This interpretation is consistent with the sudden drop of the magma column seen in summit craters on 21 January, the brief duration of the preeruptive seismic crisis, and our petrologic and geochemical evidence for a closed system (i.e., relatively fast) ascent of the erupted magma (section 5.2). Hence, we consider most plausible a tectonic trigger of the 1974 event.

[44] The rate of ascent of a magmatic intrusion depends on numerous factors, among which the structure of the crust, the stress distribution and fracture toughness of country rocks, and the intrinsic properties (initial overpressure, viscosity, density, buoyancy, volume, crystal and volatile content) of the intruding magma [e.g., *Ryan*, 1987, 1988, 1994; *Lister*, 1990; *Lister and Kerr*, 1991; *Mériaux and Jaupart*, 1998; *McLeod and Tait*, 1999; *Gudmunsson*, 2002; *Woods et al.*, 2006]. For the sake of simplicity, here we assume that the intrusion that fed the

1974 eruption could propagate along the 70° dipping focal plane defined by the most energetic and best localized earthquakes that connects the 10 ± 2 km deep magma storage level to the flank eruption site (Figure 11). In such conditions, the intrusion would have had a "vertical" extent ($h$) of ~13 km and could have propagated at a mean rate of $1.7 \times 10^{-2}$ m s$^{-1}$ during the 9 days between the first major earthquakes at that depth (21 January) and the eruption onset. A comparable rate was inferred for magma intrusion prior to the 2001 eruption, even though from a shallower (~3 km bsl) source depth [*Patanè et al.*, 2002]. However, because the nucleation of a dike-like intrusion may initially be a slow process [e.g., *Lister and Kerr*, 1991; *Mériaux and Jaupart*, 1998; *McLeod and Tait*, 1999], the above mean values provide a lower bound for the actual magma rise speed.

[45] In order to get more quantitative constraints, we have computed the gas volume fraction, density and viscosity of the 1974 trachybasaltic magma during closed system decompression from 10 km lithostatic depth bsl, for an initial temperature of 1140°C, a mean water content of 3.2 wt % and 1.5 wt % of initial coexisting gas phase (Figure 10). Neglecting its very low crystal content, the viscosity $\mu_m$ and density $\rho_m$ of the magma-volatile mixture essentially depend on the P-related evolution of the melts water content and the gas volume fraction $\alpha$. The latter was found to increase from 17% at 300 MPa (or ~12% at 400 MPa) to 77% at 10 MPa (suggesting that magma fragmentation could have begun within the upper few hundred meters of the dike-like intrusion). For such high gas volume fractions, $\mu_m \cong \mu_L*(1-\alpha)^{-5/2}$ [*Jaupart and Vergniolle*, 1989], where $\mu_L$ is the viscosity (~2 Pa s) of the vesicle-free water-rich 1974 melt computed from the equation of *Giordano and Dingwell* [2003]. The trachybasaltic magma thus increased in viscosity from 2.8 Pa s at 300 MPa to 82 Pa s at 10 MPa (or about 100 Pa s if we also take account of its cooling from 1140 to ~1080°C; section 4.3). In the same time, its density contrast ($\Delta\rho$) with respect to the host rock units cut by the intrusion increased from 380 to 2050 kg m$^{-3}$. Therefore, the magma was increasingly gas-rich and buoyant upon ascent, and could have accelerated upward.

[46] Now, maintaining closed system ascent of such a magma up to shallow depths requires typical rise speeds of order 0.1–1.0 m$^3$ s$^{-1}$ [e.g., *Parfitt*, 2004], much higher than the mean propagation rate estimated above. We thus infer that the 1974 dike-like intrusion initially nucleated and propagated at a slow rate at great depths, then progressively accelerated while becoming more and more buoyant upon ascent and while cutting the softer material of the shallow Numidian flyschoid series. The half width ($w$) of the intrusion can be estimated as [e.g., *Mériaux and Jaupart*, 1998]: $w = (2*\mu*Q/3*\Delta\rho*g)^{1/3}$, where $\mu$ is the viscosity of the magma, $Q$ is its volumetric flow rate, $\Delta\rho$ is its buoyancy, and $g$ is the gravitational acceleration. Using the average eruption rate of dense magma during the whole eruption (1.8 m$^3$ s$^{-1}$; Table 1) and the above numerical values for the pressure-related evolution of $\mu$, $\Delta\rho$ and $\alpha$ (the gas volume fraction which contributes to $Q$), we infer a dike-like intrusion's width increasing from 0.2 m at 400 MPa to about 1 m at 10 MPa. We just note that dike widths of about 1 m are quite typical on Mount Etna [e.g., *Acocella and Neri*, 2003].

### 5.4. Volatile Budget of the 1974 Eruption

[47] The total amount of volatiles released into the atmosphere by the 1974 flank eruption can be quantified from its bulk magma budget ($5.4 \times 10^6$ m$^3$, or $1.5 \times 10^{10}$ kg for a trachybasalt density of 2760 kg m$^{-3}$) and the mass fraction of each volatile species released per kilogram of melt. According to olivine-hosted melt inclusions, the initial contents of water, sulfur and chlorine in the 1974 magma averaged 3.2, 0.35 and 0.2 wt %, respectively (Table 3). Residual $H_2O$ in degassed Etna lavas averages 0.2 wt % [*Métrich et al.*, 2004; *Spilliaert et al.*, 2006], and residual contents of <0.01 wt % and 0.12 wt % were measured for S and Cl, respectively, in degassed 1974 bulk rocks (equivalent to the bulk melt). Carbon dioxide is virtually totally lost upon eruption, so its degassed mass fraction equals its original content in Etna magma, inferred as > 1.5–2 wt % [*Allard et al.*, 1991; *Aiuppa et al.*, 2007]. On these grounds, we compute that the 1974 eruption emitted about $7.8 \times 10^8$ kg of total gas, consisting of $4.5 \times 10^8$ kg of $H_2O$, $2.2 \times 10^8$ kg of $CO_2$, $1.0 \times 10^8$ kg of $SO_2$ and $1.2 \times 10^7$ kg of HCl (Table 1). When averaged over the 35 days of the eruption, the emission rate of $SO_2$ (~$3 \times 10^6$ kg d$^{-1}$) is comparable to the measured mean $SO_2$ flux from the summit craters in the mid-1970s [*Allard et al.*, 1991], thus implying about a doubling of Mount Etna's sulfur emission during the flank eruption.

### 5.5. First Historical Extrusion of an Alkali-Enriched Magma Feeding Mount Etna

[48] As already mentioned, the most outstanding peculiarity of the 1974 DDF flank eruption resides in the geochemistry of its magma, which was unusually rich in alkalis compared to all magmas erupted by Mount Etna in the past centuries (pre-1970s series). In that respect, this event constitutes an important benchmark in the recent history of Etna. Indeed, it marked the first extrusion of a more radiogenic and alkali-rich basaltic magma that has recently started to supply the volcano [*Métrich et al.*, 2004; *Spilliaert et al.*, 2006]. This magma-type, best represented by the MgO richest products of the 2002–2003 DDF-type eruption, has progressively invaded the plumbing system, mixing with and replacing the former K-poor resident magma [*Métrich et al.*, 2004; *Spilliaert et al.*, 2006; *Corsaro et al.*, 2007]. As proposed by *Métrich et al.* [2004], *Spilliaert et al.* [2006], and *Corsaro et al.* [2007], these magmas are issued from genetically distinct primary melts.

[49] Our trace element and melt inclusion data for the 1974 eruption products allow us to determine the degree of mixing, at that time, between the new feeding alkali-rich magma and the former K-poor resident magmas at ~10 km depth bsl. All the erupted rocks had a homogeneous trace element content that indicates a subtle but real imprint of the pre-1970s magma. The geochemistry of the 1974 magma is well explained by homogeneous mixing between two trachybasaltic end-members that shared the same degree of evolution (Th = 7.1 ± 0.1 ppm) but differed in their alkali content (Figure 6f). Its Rb/Th ratio (6.1) constrains respective mixing proportions of 0.75:0.25 between the 2002–

2003 DDF end-member (Rb/Th = 6.9 [*Spilliaert et al.*, 2006; R. A. Corsaro, unpublished data, 2004]) and the 1763 DDF (La Montagnola) magma (Rb/Th = 3.8), the most primitive specimen of pre-1970s K-poor series. Similar mixing proportions are indicated by the $^{86}Sr/^{87}Sr$ ratio of the 1974 trachybasalt (0.703564) compared to the $^{86}Sr/^{87}Sr$ ratios of the 1763 basalt (0.703414) and the 2001–2003 aphyric trachybasalts (0.703610–0.703666) [*Tonarini et al.*, 2001; L. Civetta, personal communication, 2007]. The few melt inclusions with intermediate K/Na, K/Cl and S/Cl ratios (Figure 8) entrapped in some olivine microphenocrysts of the 1974 magma further demonstrate, at the microscale, that both K-poor and K-rich trachybasalts were able to mix together at 10 km depth bsl in the feeding system.

[50] In contrast, the products from the 1974 summit crater activity still displayed a prevalent K-poor magma imprint (Rb/Th = 4.4; Figure 6f), with a reverse mixing proportion (0.25:0.75) between the K-rich (2002–2003) and K-poor (1763) magmas. Hence, at that time, only 25% of the magma filling the central conduit system of Etna was derived from the newly feeding magma. At present, plagioclase-rich trachybasalts that typically crystallize at low pressure in the central volcano conduits, such as CCF-type lavas erupted in 2001–2003, display Rb/Th and Rb/Nb ratios equivalent to that of the 1974 DDF magma. Therefore, since the 1974 eruption the new feeding magma has gradually invaded the plumbing system at shallower depths and now contributes about 75% of the magma stored in the central conduits of Etna.

### 5.6. Forecasting 1974-Type DDF Flank Eruptions on Etna

[51] Even though DDF-type flank eruptions are much rarer than CCF-type ones at Mount Etna, the 1763, 1974, 2001, and 2002–2003 events show that these eruptions are highly explosive and can occasionally break out at low elevations and at great distances from the volcano summit. They can thus directly or indirectly (through abundant ashfallout) affect densely populated areas on and around the volcano. Therefore, being able to forecast such events is of outmost importance for hazard mitigation and civil defense management. This capability will be conditioned by the actual triggering mechanism of the event, the rate of magma migration, and the nature and duration of premonitory signals. The 1974 example, in particular, shows that tectonic fracturing of the crust may trigger magma migration and eruption from as deep as ~10 km bsl in less than 10 days, leaving little time for hazard evaluation and emergency planning. Hence, adequate monitoring tools are necessary to detect the precursors of such events.

[52] As illustrated by the 1974 event and more recent Etna flank eruptions in 1989, 2001, and 2002–2003, seismic and ground deformations monitoring are key tools for tracking magma intrusion due to either tectonic fracturing or/and magma overpressure. Also, because DDF intrusions generally use preexisting volcano-tectonic structures to reach the surface, the detailed mapping and survey of these structures is an important baseline approach. In particular, monitoring the fumaroles or diffuse gas emanations linked to these active fault systems can provide useful indications upon deep magma recharge and intrusions [e.g., *Baubron et al.*, 1991; *Aiuppa et al.*, 2004; *Giammanco et al.*, 2007]. Another interesting perspective for the forecasting of dike intrusions and flank eruptions is provided by spaceborne infrared survey of the normalized greenness index of the vegetation growing along active volcano-tectonic structures [*Houlié et al.*, 2006]. Using this tool, *Houlié et al.* [2006] detected positive greenness anomalies (i.e., increased photosynthetic activity) in plants growing along the Pernicana fault system (Figure 1a) 1 year at least prior to the 2002 flank eruption of Etna. They interpreted these anomalies as being due to precursory dike-fed intrusions or dike wedging beneath the fault system that could have modified the physicochemical properties of local soils and lead to enhanced vegetation growth.

[53] Interestingly, spaceborne infrared imaging of Etna in September 1973 revealed an analogous anomaly in the vegetation canopy (or greenness index) right on the western flank area where the 1974 flank eruption took place four months later [*Working Group for the Surveillance of Etna*, 1974]. Although poorly quantified at that time, this spectroscopic signal could be taken as a premonitory indicator of shallow dike intrusion(s) according to the interpretation of *Houlié et al.* [2006]. However, we have shown in this study that the chemical composition, mineralogy and geochemistry of the 1974 magma are by no means compatible with its possible preeruptive storage at shallow depth. Therefore, we propose instead that the greenness anomaly detected in September 1973 might have tracked precursory changes in the subsurface ground permeability and fluid circulation (water, $CO_2$) induced by microfracturing and possible microseismicity that were already initiating on the western flank of Etna four months before the January 1974 tectonic seismic crisis. In particular, because Mount Etna is a site with widespread diffuse emanations of magma-derived carbon dioxide preferentially concentrated on fault systems [*Allard et al.*, 1991; *D'Alessandro et al.*, 1997; *Aiuppa et al.*, 2004; *Giammanco et al.*, 2007], such a mechanism could have promoted enhanced $CO_2$ flux and, thereby, enhanced photosynthetic activity across the faulting area. If correct, our hypothesis could also offer an alternative explanation to the vegetation greenness anomalies on the Pernicana fault, a noneruptive but actively moving transcurrent volcano-tectonic fracture system, detected prior to Etna's 2002 flank eruption. Further investigations are clearly required to elucidate this important question, considering its applications to eruption forecasting and hazard mitigation.

## 6. Conclusions

[54] We provide a detailed study of the 1974 flank eruption of Mount Etna based on new analyses of the mineralogy, geochemistry, and volatile content of its magma. Our results have led to the following main conclusions:

[55] 1. The 1974 eruption of Etna is an archetype of "deep dike-fed" (DDF) flank eruptions which are driven by dike-like magma intrusions that originate from below the volcanic pile and bypass its central conduits. These eruptions emit nearly aphyric, plagioclase-free magma and, thus, contrast both in their genesis and their products from the more common central conduit-fed (CCF) flank eruptions.

[56] 2. The 1974 trachybasaltic magma likely rose from an intermediate magma storage zone at 10 ± 2 km depth bsl,

located at the interface between the base of the Hyblean carbonate platform and the lower crystalline basement. Magma ascent was rapid enough to preserve closed system conditions up to ~2 km depth bsl and perhaps up to the surface during the initial eruption stages, leading to lava fountains and the rapid growth of Mount De Fiore pyroclastite cones. A lower rise speed during subsequent activity favored enhanced gas-melt separation and open degassing in the upper portion of the feeding intrusion, sustaining powerful Strombolian activity and the outpouring of sluggish lava flows.

[57] 3. The spatial and temporal evolution of the preeruptive seismicity, combined with volcanological, petrological and geochemical evidence, suggests that the 1974 eruption had a prevalent tectonic trigger. Downward fracturing of the crust underlying the western half of the volcano is interpreted to have provoked a depressurization of a depressurization of the $10 \pm 2$ km deep feeding system, triggering the nucleation and then westward propagation of a dike-like intrusion along a 70° inclined pathway defined by the best localized and most energetic earthquakes.

[58] 4. The 1974 flank eruption marked the first clear output of a more alkali-rich and more radiogenic magma compared to all lavas previously erupted in historical times, evidencing the input of a newly feeding magma. It thus constitutes an important milestone in the recent evolution of Etna. The new magma, best represented by aphyric primitive products erupted during the 2002–2003 DDF-type eruption, has progressively replenished Etna's feeding system in the following decades. The 1974 trachybasalt derived from a mixing, at ~10 km depth bsl, between 75% of this new magma and 25% of the former K-poor resident magma, best represented by the 1763 La Montagnola basalt. In contrast, the products from 1974 activity at the summit craters still displayed a prevalent (75%) imprint of the K-poor resident magmas.

[59] 5. Forecasting DDF flank eruptions on Etna requires adequate detection of their forerunner signals, among which changes in gas emanations and vegetation greenness index that could result from precursory microseismicity and ground fracturing.

[60] **Acknowledgments.** The authors are indebted with R. Romano for the valuable collection of samples and information that greatly supported this research; to A. Sobolev for his invitation to analyze water in melt inclusions by SIMS at Max Planck Institute, and the Nuclear probe team in LPS for their assistance in analyzing carbon; to B. Puglisi, who kindly furnished his photos of the 1974 activity; and to L. Messina for preparing powder for rocks analyses. Most of the analyzed samples come from the Petroteca archive of Istituto Nazionale di Geofisica e Vulcanologia, in Catania. Thorough reviews by M. P. Ryan, C. Thornber, and V. S. Kamenetsky allowed significant improvement of our manuscript. This work was funded by the Italian Dipartimento della Protezione Civile in the frame of 2004–2006 Agreement with Istituto Nazionale di Geofisica e Vulcanologia.

## References

Acocella, V., and M. Neri (2003), What makes flank eruptions? The 2001 Mount Etna eruption and its possible triggering mechanisms, *Bull. Volcanol.*, *65*, 517–529, doi:10.1007/s00445-003-0280-3.

Aiuppa, A., P. Allard, W. D'Alessandro, S. Giammanco, F. Parello, and M. Valenza (2004), Magmatic gas leakage at Mount Etna (Sicily, Italy): Relationships with the volcano-tectonic structures, the hydrological pattern and the eruptive activity, in *Mt. Etna: Volcano Laboratory*, *Geophys. Monogr. Ser*, vol. 143, edited by A. Bonaccorso et al., pp. 129–145, AGU, Washington, D. C.

Aiuppa, A., R. Moretti, C. Federico, G. Giudice, S. Gurrieri, M. Liuzzo, P. Papale, H. Shinohara, and M. Valenza (2007), Forecasting Etna eruptions by real-time observation of volcanic gas composition, *Geology*, *35*(12), 1115–1118, doi:10.1130/G24149A.1.

Allard, P., et al. (1991), Eruptive and diffuse emissions of $CO_2$ from Mount Etna, *Nature*, *351*, 387–391, doi:10.1038/351387a0.

Allard, P., B. Behncke, S. D'Amico, M. Neri, and S. Gambino (2006), Mount Etna 1993–2005: Anatomy of an evolving eruptive cycle, *Earth Sci. Rev.*, *78*, 85–114, doi:10.1016/j.earscirev.2006.04.002.

Andronico, D., and L. Lodato (2005), Effusive activity at Mount Etna Volcano (Italy) during the 20th century: A contribution to volcanic hazard assessment, *Nat. Hazards*, *36*, 407–443, doi:10.1007/s11069-005-1938-2.

Andronico, D., et al. (2005), A multi-disciplinary study of the 2002–03 Etna eruption: Insights into a complex plumbing system, *Bull. Volcanol.*, *67*, 314–330, doi:10.1007/s00445-004-0372-8.

Armienti, P., F. Innocenti, R. Petrini, M. Pompilio, and L. Villari (1988), Sub-aphyric alkali basalt from Mt. Etna: Inferences on the depth and composition of the source magma, *Bull. Mineral. Rend. Soc. Ital. Mineral. Petrol.*, *43*, 877–891.

Armienti, P., S. Tonarini, M. D'Orazio, and F. Innocenti (2004), Genesis and evolution of Mt. Etna alkaline lavas: Petrological and Sr-Nd-B isotope constraints, *Period. Mineral.*, *73*, 29–52.

Baubron, J. C., P. Allard, J. C. Sabroux, D. Tedesco, and J. P. Toutain (1991), Soil gas emanations as precursory indicators of volcanic eruptions, *J. Geol. Soc.*, *148*, 571–576, doi:10.1144/gsjgs.148.3.0571.

Bonaccorso, A., and P. M. Davis (2004), Modeling of ground deformation associated with recent lateral eruptions: Mechanics of magma ascent and intermediate storage at Mt. Etna, in *Mt. Etna: Volcano Laboratory*, *Geophys. Monogr. Ser*, vol. 143, edited by A. Bonaccorso et al., pp. 293–320, AGU, Washington, D. C.

Bottari, A., E. Lo Giudice, G. Patanè, R. Romano, and C. Sturiale (1975), L'eruzione etnea del Gennaio-Marzo 1974, *Riv. Miner. Siciliana*, *154–156*, 175–199.

Branca, S., and P. Del Carlo (2004), Eruptions of Mt. Etna during the past 3200 years: A revised compilation integrating the historical and stratigraphic records, in *Mt. Etna: Volcano Laboratory*, *Geophys. Monogr. Ser*, vol. 143, edited by A. Bonaccorso et al., pp. 1–27, AGU, Washington, D. C.

Carignan, J., P. Hild, G. Mevelle, J. Morel, and D. Yeghicheyan (2001), Routine analyses of trace elements in geological samples using flow injection and low pressure on-line liquid chromatography coupled to ICP-MS: A study of geochemical reference materials BR, DR-N, UB-N, AN-G and GH, *Geostand. Newsl.*, *25*, 187–198, doi:10.1111/j.1751-908X.2001.tb00595.x.

Castellano, M., F. Ferrucci, C. Godano, S. Imposa, and G. Milano (1993), Upwards migration of seismic focii: A forerunner of the 1989 eruption of Mt Etna (Italy), *Bull. Volcanol.*, *55*, 357–361, doi:10.1007/BF00301146.

Chester, D. K., A. M. Duncan, J. E. Guest, and C. R. J. Kilburn (1985), *Mount Etna, the Anatomy of a Volcano*, Chapman and Hall, London.

Chiarabba, C., A. Amato, E. Boschi, and F. Barberi (2000), Recent seismicity and tomographic modeling of the Mount Etna plumbing system, *J. Geophys. Res.*, *105*, 10,923–10,938, doi:10.1029/1999JB900427.

Chiarabba, C., P. De Gori, and D. Patanè (2004), The Mt. Etna plumbing system: The contribution of seismic tomography, in *Mt. Etna: Volcano Laboratory*, *Geophys. Monogr. Ser*, vol. 143, edited by A. Bonaccorso et al., pp. 191–204, AGU, Washington, D.C.

Clocchiatti, R., J. L. Joron, and M. Treuil (1988), The role of selective alkali contamination in the evolution of recent historic lavas of Mt. Etna, *J. Volcanol. Geotherm. Res.*, *34*, 241–249, doi:10.1016/0377-0273(88)90036-4.

Clocchiatti, R., M. Condomines, N. Guénot, and J. C. Tanguy (2004), Magma changes at Mount Etna: The 2001 and 2002–2003 eruptions, *Earth Planet. Sci. Lett.*, *226*, 397–414, doi:10.1016/j.epsl.2004.07.039.

Coltelli, M., P. Del Carlo, M. Pompilio, and L. Vezzoli (2005), Explosive eruption of a picrite: The 3930 BP subplinian eruption of Etna volcano (Italy), *Geophys. Res. Lett.*, *32*, L23307, doi:10.1029/2005GL024271.

Condomines, M., R. Bouchez, J. L. Ma, J. C. Tanguy, J. Amossé, and M. Piboule (1987), Short-lived radioactive disequilibria and magma dynamics in Etna volcano, *Nature*, *325*, 607–609, doi:10.1038/325607a0.

Condomines, M., J. C. Tanguy, and V. Michaud (1995), Magma dynamics at Mt. Etna: Constraints from U-Th-Ra-Pb radioactive disequilibria and Sr isotopes in historical lavas, *Earth Planet. Sci. Lett.*, *132*, 25–41, doi:10.1016/0012-821X(95)00052-E.

Corsaro, R. A., and M. Pompilio (2004), Magma dynamics in the shallow plumbing system of Mt. Etna as recorded by compositional variations in volcanics of recent summit activity (1995–1999), *J. Volcanol. Geotherm. Res.*, *137*(1–3), 55–71, doi:10.1016/j.jvolgeores.2004.05.008.

Corsaro, R. A., L. Miraglia, and M. Pompilio (2007), Petrologic evidence of a complex plumbing system feeding the July August 2001 eruption of

Mt. Etna, Sicily, Italy, *Bull. Volcanol.*, *69*, 401–421, doi:10.1007/s00445-006-0083-4.
Couch, S., R. S. J. Sparks, and M. R. Carroll (2003), The kinetics of degassing-induced crystallization at Soufrière Hills volcano, Montserrat, *J. Petrol.*, *44*, 1477–1502, doi:10.1093/petrology/44.8.1477.
D'Alessandro, W., S. Giammanco, F. Parello, and M. Valenza (1997), $CO_2$ output and $\delta^{13}C$ ($CO_2$) from Mount Etna as indicators of degassing of shallow asthenosphere, *Bull. Volcanol.*, *58*, 455–458, doi:10.1007/s004450050154.
Dixon, J. E. (1997), Degassing of alkalic basalts, *Am. Mineral.*, *82*, 368–378.
Downes, M. J. (1974), Sector and oscillatory zoning of calcic augites from M. Etna, Sicily, *Contrib. Mineral. Petrol.*, *142*, 261–283.
Frezzotti, M. L., B. De Vivo, and R. Clocchiatti (1991), Melt-mineral-fluid interactions in ultramafic nodules from alkaline lavas of M.Etna (Sicily, Italy): Melt and fluid inclusion evidence, *J. Volcanol. Geotherm. Res.*, *47*, 209–219, doi:10.1016/0377-0273(91)90001-G.
Giammanco, S., K. W. W. Sims, and M. Neri (2007), Measurements of $^{220}Rn$ and $^{222}Rn$ and $CO_2$ emissions in soil and fumarole gases on Mt. Etna volcano (Italy): Implications for gas transport and shallow ground fracture, *Geochem. Geophys. Geosyst.*, *8*, Q10001, doi:10.1029/2007GC001644.
Giordano, D., and D. B. Dingwell (2003), Viscosity of hydrous Etna basalt: Implications for Plinian-style basaltic eruptions, *Bull. Volcanol.*, *65*, 8–14.
Gudmunsson, A. (2002), Emplacement and arrest of sheets and dykes in central volcanoes, *J. Volcanol. Geotherm. Res.*, *116*, 279–298, doi:10.1016/S0377-0273(02)00226-3.
Guerra, I., A. Lo Bascio, G. Luongo, and R. Scarpa (1976), Seismic activity accompanying the 1974 eruption of Mt. Etna, *J. Volcanol. Geotherm. Res.*, *1*, 347–362, doi:10.1016/0377-0273(76)90024-X.
Guest, J. E., A. T. Huntington, G. Wadge, G. Brander, B. Booth, S. Carter, and A. Duncan (1974), Recent eruption of Mount Etna, *Nature*, *250*, 385–387, doi:10.1038/250385a0.
Hirn, A., A. Nercessian, M. Sapin, F. Ferrucci, and G. Wittlinger (1991), Seismic heterogeneity of Mt. Etna: Structure and activity, *Geophys. J. Int.*, *105*, 139–153, doi:10.1111/j.1365-246X.1991.tb03450.x.
Houlié, N., J. C. Komorowski, M. de Michele, M. Kasereka, and H. Ciraba (2006), Early detection of eruptive dykes revealed by normalized difference vegetation index (NDVI) on Mt. Etna and Mt. Nyiragongo, *Earth Planet. Sci. Lett.*, *246*, 231–240, doi:10.1016/j.epsl.2006.03.039.
Jarosewich, E., J. A. Nelen, and J. A. Norberg (1980), Reference samples for electron microprobe analysis, *Geostand. Newsl.*, *4*, 43–47, doi:10.1111/j.1751-908X.1980.tb00273.x.
Jaupart, C., and S. Vergniolle (1989), The generation and collapse of foam layer at the roof of a basaltic magma chamber, *J. Fluid Mech.*, *203*, 347–380, doi:10.1017/S0022112089001497.
Joron, J. L., and M. Treuil (1984), Etude géochimique et pétrogenèse des laves de l'Etna, Sicile, Italie, *Bull. Volcanol.*, *47*, 1125–1144, doi:10.1007/BF01952368.
Kamenetsky, V., and R. Clocchiatti (1996), Primitive magmatism of Mt. Etna: Insights from mineralogy and melt inclusions, *Earth Planet. Sci. Lett.*, *142*, 553–572, doi:10.1016/0012-821X(96)00115-X.
Kamenetsky, V., M. Pompilio, N. Métrich, A. Sobolev, D. Kuzmin, and R. Thomas (2007), Deep supply of volatile-rich high-Mg magmas changes explosivity of Mount Etna eruptions, *Geology*, *35*(3), 255–258, doi:10.1130/G23163A.1.
Le Maitre, R. W. (Ed.) (2002), *Igneous Rocks: A Classification and Glossary of Terms, Recommendations of the IUGS Subcomission on the Systematics of Igneous Rocks*, 2nd ed., 236 pp., Cambridge Univ. Press, Cambridge, U. K.
Lentini, F. (1982), The geology of the Mt. Etna basement, *Mem. Soc. Geol. Ital.*, *23*, 7–25.
Lister, J. R. (1990), Buoyancy-driven fluid fracture: Effects of material roughness and of low-viscosity precursors, *J. Fluid Mech.*, *210*, 263–280, doi:10.1017/S0022112090001288.
Lister, J. R., and R. C. Kerr (1991), Fluid-mechanical models of crack propagation and their application to magma transport in dikes, *J. Geophys. Res.*, *96*, 10,049–10,077, doi:10.1029/91JB00600.
Mazzarini, F., and P. Armienti (2001), Flank cones at Mount Etna volcano: Do they have a power law distribution?, *J. Volcanol. Geotherm. Res.*, *62*, 420–430.
McLeod, P., and S. Tait (1999), The growth of dykes from magma chambers, *J. Volcanol. Geotherm. Res.*, *92*, 231–245, doi:10.1016/S0377-0273(99)00053-0.
Mériaux, C., and C. Jaupart (1998), Dike propagation through an elastic plate, *J. Geophys. Res.*, *103*, 18,295–18,314, doi:10.1029/98JB00905.
Métrich, N., and M. J. Rutherford (1998), Low pressure crystallization paths of H2O-saturated basaltic-hawaiitic melts from Mt. Etna: Implications for open-system degassing volcanoes, *Geochim. Cosmochim. Acta*, *62*, 1195–1205, doi:10.1016/S0016-7037(98)00048-9.
Métrich, N., P. Allard, N. Spilliaert, D. Andronico, and M. Burton (2004), 2001 flank eruption of the alkali and volatile-rich primitive basalt responsible for Mount Etna's evolution in the last three decades, *Earth Planet. Sci. Lett.*, *228*, 1–17, doi:10.1016/j.epsl.2004.09.036.
Miraglia, L. (2002), Evidence for heterogeneous magmas in the feeding system of the 1763 "La Montagnola" eruption at Mount Etna, *Plinius*, *27*, 108–112.
Miraglia, L. (2006), Valutazione dell'accuratezza e della precisione delle analisi eseguite con il sistema analitico SEM-EDS su standard internazionali di minerali e vetri, *Rep. UFVG2006/115*, 5 pp., Ist. Naz. Geofis. e Vulcanol., Catania, Italy.
Murru, M., C. Montuori, M. Wyss, and E. Privitera (1999), The location of magma chambers at Mt. Etna, Italy, mapped by b-values, *Geophys. Res. Lett.*, *26*, 2553–2556, doi:10.1029/1999GL900568.
Newman, S., and J. B. Lowenstern (2002), VOLATILECALC: A silicate melt-$H_2O$-$CO_2$ solution model written in Visual Basic Excel, *Comput. Geosci.*, *28*, 597–604, doi:10.1016/S0098-3004(01)00081-4.
Papale, P., R. Moretti, and D. Barbato (2006), The compositional dependence of the saturation surface of $H_2O$ + $CO_2$ fluids in silicate melts, *Chem. Geol.*, *229*, 78–95, doi:10.1016/j.chemgeo.2006.01.013.
Parfitt, E. A. (2004), A discussion of the mechanisms of explosive basaltic eruptions, *J. Volcanol. Geotherm. Res.*, *134*, 77–107, doi:10.1016/j.jvolgeores.2004.01.002.
Patanè, D., C. Chiarabba, O. Cocina, P. De Gori, M. Moretti, and E. Boschi (2002), Tomographic images and 3D earthquake locations of the seismic swarm preceding the 2001 Mt. Etna eruption: Evidence for a dyke intrusion, *Geophys. Res. Lett.*, *29*(10), 1497, doi:10.1029/2001GL014391.
Pompilio, M., R. Trigila, and V. Zanon (1998), Melting experiments on Mt. Etna lavas: I-The calibration of an empirical geothermometer to estimate the eruptive temperature, *Acta Vulcanol.*, *10*(1), 67–75.
Riedel, C., G. G. J. Ernst, and M. Riley (2003), Controls on the growth and geometry of pyroclastic constructs, *J. Volcanol. Geotherm. Res.*, *127*, 121–152, doi:10.1016/S0377-0273(03)00196-3.
Rittmann, A. (1965), Notizie sull'Etna, *Suppl. Nuovo Cimento*, *3*(I), 1117–1123.
Rittmann, A., R. Romano, and C. Sturiale (1971), L'eruzione etnea dell'aprile–giugno 1971, *Atti Accad. Gioenia Sci. Nat.*, *VII*, 3–29.
Romano, R., and C. Sturiale (1982), The historical eruptions of Mt. Etna (volcanological data), *Mem. Soc. Geol. Ital.*, *23*, 75–98.
Ryan, M. P. (1987), Neutral buoyancy and the mechanical evolution of magmatic systems, in *Magmatic Processes: Physicochemical Principles*, edited by B. O. Mysen, *Geochem. Soc. Spec. Publ.*, *1*, 259–288.
Ryan, M. P. (1988), The mechanics and three-dimensional internal structure of active magmatic systems: Kilauea Volcano, Hawaii, *J. Geophys. Res.*, *93*, 4213–4248, doi:10.1029/JB093iB05p04213.
Ryan, M. P. (1994), Neutral buoyancy-controlled magma transport and storage in mid-ocean ridge magma reservoirs and their sheeted dike complex: A summary of basic relationships, in *Magmatic Systems*, edited by M. P. Ryan, pp. 97–135, Academic, San Diego, Calif.
Schiano, P., R. Clocchiatti, L. Ottolini, and T. Busà (2001), Transition of Mount Etna lavas from a mantle-plume to an island-arc magmatic source, *Nature*, *412*, 900–904, doi:10.1038/35091056.
Sobolev, A., and M. Chaussidon (1996), $H_2O$ concentrations in primary melts from supra-subduction zones and mid-ocean ridges: Implications for $H_2O$ storage and recycling in the mantle, *Earth Planet. Sci. Lett.*, *137*, 45–55, doi:10.1016/0012-821X(95)00203-O.
Spilliaert, N., P. Allard, N. Métrich, and A. V. Sobolev (2006), Melt inclusion record of the conditions of ascent, degassing, and extrusion of volatile-rich alkali basalt during the powerful 2002 flank eruption of Mount Etna (Italy), *J. Geophys. Res.*, *111*, B04203, doi:10.1029/2005JB003934.
Sturiale, C. (1970), La singolare eruzione dell'Etna del 1763 "La Montagnola", *Bull. Mineral. Rend. Soc. Ital. Mineral. Petrol.*, *26*, 314–351.
Tanguy, J. C. (1980), L'Etna: Etude pétrologique et paléomagnétique. Implications volcanologiques, thesis, 618 pp., Univ. Pierre et Marie Curie Paris 6, Paris, 15 Dec.
Tanguy, J. C., and G. Kieffer (1977), The 1974 eruption of Mount Etna, *Bull. Volcanol.*, *40*(4), 239–252, doi:10.1007/BF02597566.
Tanguy, J. C., M. Condomines, and G. Kieffer (1997), Evolution of the Mount Etna magma: Constraints on the present feeding system and eruptive mechanism, *J. Volcanol. Geotherm. Res.*, *75*, 221–250, doi:10.1016/S0377-0273(96)00065-0.
Tazieff, H. (1974), Card 1791, 06/1974, *Bulletin of the Global Volcanic Network*, Smithson. Inst., Washington, D. C.
Tonarini, S., P. Armienti, M. D'Orazio, and F. Innocenti (2001), Subduction-like fluids in the genesis of Mt. Etna magmas: Evidence from boron

isotopes and fluid mobile elements, *Earth Planet. Sci. Lett.*, *192*, 471–483, doi:10.1016/S0012-821X(01)00487-3.

Viccaro, M., C. Ferlito, L. Cortesogno, R. Cristofolini, and L. Gaggero (2006), Magma mixing during the 2001 event at Mount Etna (Italy): Effects on the eruptive dynamics, *J. Volcanol. Geotherm. Res.*, *149*, 139–159, doi:10.1016/j.jvolgeores.2005.06.004.

Wadge, G. (1980), Flank fissures of Etna and the surface expressions of magmatic conduits, in *United Kingdom Research on Mount Etna 1977–79*, pp. 27–30, R. Soc., London.

Woods, A. W., O. Bokhove, A. de Boer, and B. E. Hill (2006), Compressible magma flow in a two-dimensional elastic-walled dike, *Earth Planet. Sci. Lett.*, *246*, 241–250, doi:10.1016/j.epsl.2005.11.065.

Working Group for the Surveillance of Etna (1974), Summary report on the 1974 Etna eruption, *Open File Rep. 68*, Ist. Int. di Vulcanol., CNR, Catania, Italy.

P. Allard and N. Métrich, Laboratoire Pierre Süe, UMR 9956, CEA, CE-Saclay, CNRS, F-91191 Gif-sur-Yvette, France. (patrick.allard@cea.fr; nicole.metrich@cea.fr)

D. Andronico, R. A. Corsaro, and L. Miraglia, Istituto Nazionale di Geofisica e Vulcanologia, Sezione di Catania, Piazza Roma 2, I-95123 Catania, Italy. (andronico@ct.ingv.it; corsaro@ct.ingv.it; miraglia@ct.ingv.it)

C. Fourmentraux, Dipartimento di Scienze della Terra, Via Santa Maria 53, I-56126 Pisa, Italy. (cfourmentraux@dst.unipi.it)